INTERNATIONAL JOURNAL OF
NUMERICAL ANALYSIS AND MODELING
Volume 22, Number 3, Pages 307–339

doi: 10.4208/ijnam2025-1014

A LOCKING-FREE REDUCED-ORDER MODEL FOR SOLVING THE ELASTIC WAVE EQUATION

LU WANG, YOUCAI XU, AND MINFU FENG*

Abstract. In this paper, a new locking-free mixed full-order model (FOM) for solving the elastic wave equation is studied, and then a locking-free reduced-order model (ROM) based on the proper orthogonal decomposition (POD) technique is constructed, which greatly improves solving efficiency compared to FOM while maintaining the locking-free. Theoretical analysis of semi discrete and fully discrete schemes for the FOM and the ROM are also presented. Some numerical experiments verify the theoretical analysis results.

Key words. Elastic wave equation, mixed finite element method, proper orthogonal decomposition, locking free, implicit scheme, reduced-order model.

1. Introduction

The elastic wave equation, also known as the elastodynamic equation, can be used to simulate the propagation of waves in heterogeneous media and predict damage patterns caused by earthquakes [1]. To solve the elastic wave equation, there are many various numerical methods developed, such as the finite difference (FD) method [2] and the finite element (FE) method. Owing to the advantages of dealing with complex geometry and boundary conditions, the FE method is widely used for solving the elastic wave equation. Various FE methods have been developed, including conforming finite element methods [3, 4], spectral finite element methods [5], non-conforming finite element methods [6], and discontinuous Galerkin (DG) methods [7, 8, 9].

The elastic wave equation can be viewed as a nonstationary linear elasticity problem. The classical FE method poses two challenges when solving it. One is low computational efficiency, and the other is the locking phenomenon that occurs when $\lambda \to \infty$. Developing algorithms that can simultaneously overcome and improve both of the two problems is interesting.

In terms of improving computing efficiency, the ROM based on the POD method (POD-ROM) [10, 11, 12, 13] is an effective way. This method provides an orthogonal basis for describing a given dataset in the least-squares optimal sense, enabling us to determine the best low-dimensional approximation for a particular data collection. There have been successful attempts at POD-ROM for Navier-Stokes equation [14], Stokes equation [15], parabolic equations [16], and many other problems [17]. The results of such attempts have shown that ROM can significantly enhance computational efficiency while maintaining the accuracy of the models. Some research has also been carried out on ROM for wave equations, such as [18, 19]. As far as we know, there is little research on ROM for the elastic wave equation (1).

To make the ROM meet the locking-free property when solving (1), constructing a locking-free FOM is necessary. There are some methods to be locking-free, including the mixed finite element (MFE) method. Multiple types of MFE methods

Received by the editors on April 7, 2024 and, accepted on November 4, 2024.
2000 *Mathematics Subject Classification.* 35R35, 49J40, 60G40.
*Corresponding author.

have been developed for (1), such as the MFE method based on "stress displacement" [20, 21] and "stress velocity" [22, 23] mixed form. However, for the MFE methods mentioned above, the construction of the MFE space needs to satisfy the inf-sup condition and the construction of the stress space is complicated since the symmetry of the stress must be satisfied; otherwise, a new variable with weakly applied symmetry must be introduced.

In this paper, we construct an FOM using the MFE method of "displacement pseudo-pressure" by introducing pseudo-pressure $p = \lambda \nabla \cdot \boldsymbol{u}$, and we employ an unconditionally stable implicit scheme on time discretization. The constructed mixed form is similar to the Stokes problem; as a result, some stable MFE spaces that satisfy the inf-sup condition, applicable to the Stokes problem, can also be applied to (1) [24]. Then we construct a ROM based on the FOM using the POD technique and give analysis. The results show that the POD-ROM can improve efficiency compared with the FOM and keep locking-free.

Compared to the work of [25], our method differs in the following points. Firstly, the reference only considers the case $\mu = 0$, which is the acoustic wave equation, whereas we focus on the case $\mu \neq 0$. Secondly, the reference provides an error estimate of p that is dependent on $\lambda^{-1/2}$, we improved it in our analysis. Thirdly, the reference uses an explicit, fully discrete scheme, and we use the implicit scheme. Fourthly, we further propose a ROM to improve computational efficiency.

The remainder of this paper is structured as follows: Section 2 provides an overview of the elastic wave equation and the notions and conclusions used in the subsequent theoretical analysis. Section 3 constructs the FOM by the MFE method. In Section 4, we establish the POD-ROM and provide the algorithm. In Section 5, we validate the theoretical analysis of the FOM through some numerical tests. Section 6 provides a summary of the whole paper.

2. Preliminaries

This section presents some preliminaries of the elastic wave equation.

2.1. The mixed form of the elastic wave equation. In this section, we will discuss the mixed form of the elastic wave equation, along with some concepts and lemmas that will be used in the subsequent analysis.

Specifically, this paper will focus on the elastic wave equation in either two or three dimensions. Let $\Omega \subset \boldsymbol{R}^d, (d = 2, 3)$ denotes an open, bounded, connected domain with a Lipschitz continuous boundary $\partial\Omega$. We give a body exterior force $\boldsymbol{f}$, and the elastic wave model seeks a displacement vector field $\boldsymbol{u}(\boldsymbol{x}, t) = (u_x(\boldsymbol{x}, t), u_y(\boldsymbol{x}, t))$ in two dimensions (or $\boldsymbol{u}(\boldsymbol{x}, t) = (u_x(\boldsymbol{x}, t), u_y(\boldsymbol{x}, t), u_z(\boldsymbol{x}, t))$ in three dimensions) at time t that satisfies the following equation.

$$\rho \frac{\partial^2 \boldsymbol{u}}{\partial t^2} - \nabla \cdot \sigma(\boldsymbol{u}) = \boldsymbol{f} \quad \text{in } \Omega, \tag{1}$$

where $\sigma(\boldsymbol{u})$ is the symmetric stress tensor and ρ denotes the density for linear, homogeneous, and isotropic materials. For simplicity, we assume that the density ρ is a constant. The stress tensor $\sigma(\boldsymbol{u})$ is related to the strain tensor by Hooke's law

$$\sigma(\boldsymbol{u}) = 2\mu\varepsilon(\boldsymbol{u}) + \lambda(\nabla \cdot \boldsymbol{u})\mathbf{I}, \tag{2}$$

where the strain tensor $\varepsilon(\boldsymbol{u})$ is

$$\varepsilon(\mathbf{u}) = \frac{1}{2}\left(\nabla \mathbf{u} + \nabla \mathbf{u}^T\right), \tag{3}$$

and the Lam constants λ and μ are given by

$$\lambda = \frac{E\tau}{(1+\tau)(1-2\tau)}, \quad \mu = \frac{E}{2(1+\tau)},$$

where E is the elasticity modulus and τ is the Poisson's ratio. Substituting (2) and (3) into (1) and eliminating stress and strain, we have the following primal form of the elastic wave equation

$$\rho\frac{\partial^2 \boldsymbol{u}}{\partial t^2} - \nabla((\lambda+\mu)\nabla\cdot\boldsymbol{u}) - \nabla\cdot(\mu\nabla\boldsymbol{u}) = \boldsymbol{f}. \tag{4}$$

There are some kinds of mixed forms of the elastic wave equation, for example, "displacement-stress" or "velocity-stress" formulations. In this paper, we study another "displacement pseudo-pressure" mixed form of the elastic wave equation by introducing a pseudo-pressure variable $p = \lambda\nabla\cdot\boldsymbol{u}$, which is like a generalized nonstationary Stokes system as follows:

$$\begin{cases} \rho\dfrac{\partial^2 \boldsymbol{u}}{\partial t^2} - 2\mu\nabla\cdot(\varepsilon(\boldsymbol{u})) - \nabla p = \boldsymbol{f}, \\ p = \lambda\nabla\cdot\boldsymbol{u}. \end{cases} \tag{5}$$

The content of the following paper relies on (5).

2.2. Notions and notations. First, we define the L^2 inner product over Ω as usual: $(u,v) = \int_\Omega uvd\Omega$, and define $\|\cdot\|_{L^2}$ as the L^2 norm over Ω, i.e., $\|u\|_{L^2(\Omega)} = (u,u)^{\frac{1}{2}}$. For a bounded domain Ω, we set $H^m(\Omega)(m \geq 0)$ and $L^2(\Omega) = H^0(\Omega)$ as the usual Sobolev spaces equipped with the semi-norm $|\cdot|_{m,\Omega}$ and the norm $\|\cdot\|_{m,\Omega}$, respectively. $\|\cdot\|_1$ is equivalent to $|\cdot|_1$ in $H_0^1(\Omega)$, where the subspace $H_0^1(\Omega)$ of $H^1(\Omega)$ is denoted as

$$H_0^1(\Omega) = \left\{u \in H^1(\Omega);\, u|_{\partial\Omega} = 0\right\}.$$

In addition, it is essential to give the Sobolev spaces dependent on time t. Let Φ be a Hilbert space. For all $T > 0$ and a integer $n \geq 0$, $H^n([0,T];\Phi)$ is defined as

$$H^n([0,T];\Phi) = \left\{v(t) \in \Phi; \int_0^T \sum_{i=0}^n \left\|\frac{\mathrm{d}^i}{\mathrm{d}t^i}v(t)\right\|_\Phi^2 \,\mathrm{d}t < \infty\right\} \quad \forall t \in [0,T],$$

equipped with the norm

$$\|u\|_{H^n([0,T];\Phi)} = \left[\sum_{i=0}^n \int_0^T \left\|\frac{\mathrm{d}^i}{\mathrm{d}t^i}u(t)\right\|_\Phi^2 \,\mathrm{d}t\right]^{\frac{1}{2}} \quad \text{for } u \in H^n([0,T];\Phi),$$

where $\|\cdot\|_\Phi$ is the norm of space Φ. Especially, if $n = 0$, the time-space norm $\|\cdot\|_{L^2([0,T];L^2(\Omega))}$ is defined as

$$\|u\|_{L^2([0,T];L^2(\Omega))} = \|u\|_{L^2(L^2)} = \left(\int_0^T \|u\|_{L^2(\Omega)}^2\right)^{\frac{1}{2}},$$

in addition, the time-space norm $\|\cdot\|_{L^\infty(L^2)}$ is similarly defined as

$$L^\infty([0,T];\Phi) = \left\{v(t) \in \Phi; \operatorname*{esssup}_{0\leq t\leq T}\|v(t)\|_\Phi < \infty\right\},$$

equipped with the norm

$$\|v\|_{L^\infty(\Phi)} = \operatorname*{esssup}_{0\leq t\leq T}\|v(t)\|_\Phi.$$

We also defined the discrete l^∞-norm for time-discrete functions $v^n = v(t_n)$ by

$$\|v\|_{l^\infty(\Phi)} = \max_{0\le n\le N} \|v^n\|_\Phi,$$

where N is the number of time domain partitions, the l^∞-norm will be used in the analysis of the fully discrete scheme.

3. The FOM constructed by the MFE method

In this section, we are going to constrcut FOM by MFE method.

3.1. The weak form. The initial boundary value problem for the mixed form of elastic wave equations (5) is as follows:

$$\begin{cases} \rho\dfrac{\partial^2 \boldsymbol{u}}{\partial t^2} - 2\mu\nabla\cdot(\varepsilon(\boldsymbol{u})) - \nabla p = \boldsymbol{f} \text{ in } \Omega\times(0,T], \\ p = \lambda\nabla\cdot\boldsymbol{u} \text{ in } \Omega\times(0,T], \\ \boldsymbol{u}(\boldsymbol{x},t) = 0 \text{ on } \partial\Omega\times(0,T], \\ \boldsymbol{u}(\boldsymbol{x},0) = \boldsymbol{u}_0 \text{ in } \Omega, \\ \boldsymbol{u}_t(\boldsymbol{x},0) = \boldsymbol{u}_1 \text{ in } \Omega, \end{cases} \tag{6}$$

where $\boldsymbol{u}_0$ and $\boldsymbol{u}_1$ are initial values of $\boldsymbol{u}$.

We first define the spaces $U = \left[H_0^1(\Omega)\right]^d$ and $M = L^2(\Omega)$. Then the weak form is generated by multiplying the test function on both sides of (6) and utilizing Green's formula: find $\boldsymbol{u} \in H^2([0,T];U)$ and $p \in L^2([0,T];M)$ such that for $\forall t \in [0,T]$:

$$\begin{cases} (\rho\dfrac{\partial^2 \boldsymbol{u}}{\partial t^2}, \boldsymbol{v}) + 2(\mu\varepsilon(\boldsymbol{u}), \varepsilon(\boldsymbol{v})) + (\nabla\cdot\boldsymbol{v}, p) = (\boldsymbol{f}, \boldsymbol{v}) \quad \forall \boldsymbol{v} \in U, \\ (\nabla\cdot\boldsymbol{u}, q) - \left(\lambda^{-1}p, q\right) = 0 \quad \forall q \in M, \\ (\boldsymbol{u}(\boldsymbol{x},0), \boldsymbol{v}) = (\boldsymbol{u}_0, \boldsymbol{v}), \\ (\boldsymbol{u}_t(\boldsymbol{x},0), \boldsymbol{v}) = (\boldsymbol{u}_1, \boldsymbol{v}), \\ (p(\boldsymbol{x},0), q) = (p_0, q). \end{cases} \tag{7}$$

Then the existence and uniqueness of the solution of (7) hold.

Lemma 3.1. *The solution $(\boldsymbol{u}, p)$ of (7) exists and is unique.*

Proof. By the similar argument of Lemma 3.1 in [25], we can draw conclusions. □

3.2. Semi discrete scheme. Following that, we will show the finite element approximation of (7). Any finite element suitable for the Stokes problem would theoretically provide a solution to (7). For example, the Taylor-Hood element and Mini element. The difference is that (7) solves a saddle-point problem with an additional pseudo-pressure variable, and it is a kind of hyperbolic equation. For simplicity of expression, first, we rewrite (7) as: find $\boldsymbol{u} \in H^2([0,T];U)$ and $p \in L^2([0,T];M)$ such that for almost all $t \in [0,T]$:

$$\begin{cases} (\rho\dfrac{\partial^2 \boldsymbol{u}}{\partial t^2}, \boldsymbol{v}) + a(\boldsymbol{u}, \boldsymbol{v}) + b(p, \boldsymbol{v}) = (\boldsymbol{f}, \boldsymbol{v}) \quad \forall \boldsymbol{v} \in U, \\ b(\boldsymbol{u}, q) - c(p, q) = 0 \quad \forall q \in M, \\ (\boldsymbol{u}(0), \boldsymbol{v}) = (\boldsymbol{u}_0, \boldsymbol{v}), \\ (\boldsymbol{u}_t(0), \boldsymbol{v}) = (\boldsymbol{u}_1, \boldsymbol{v}), \\ (p(0), q) = (p_0, q), \end{cases} \tag{8}$$

where $a(\boldsymbol{u},\boldsymbol{v})=2\mu\int_\Omega \varepsilon(\boldsymbol{u}):\varepsilon(\boldsymbol{v})\mathrm{d}\boldsymbol{x}$, $b(p,\boldsymbol{v})=\int_\Omega \nabla\cdot\boldsymbol{v}p\mathrm{d}\boldsymbol{x}$ and $c(p,q)=\lambda^{-1}\int_\Omega pq\mathrm{d}\boldsymbol{x}$.

In addition, the bilinear forms $a(\cdot,\cdot)$ and $c(\cdot,\cdot)$ have the following properties of conercivity and continuity[24]

$$a(\boldsymbol{v},\boldsymbol{v})\geq 2\mu\|\boldsymbol{v}\|_U^2 \quad \forall \boldsymbol{v}\in U, \tag{9}$$

$$|a(\boldsymbol{u},\boldsymbol{v})|\leq 2\mu\|\boldsymbol{u}\|_U\|\boldsymbol{v}\|_U \quad \forall \boldsymbol{u},\boldsymbol{v}\in U, \tag{10}$$

$$c(q,q)\geq \lambda^{-1}\|q\|_M^2 \quad \forall q\in M, \tag{11}$$

$$|c(p,q)|\leq \lambda^{-1}\|p\|_M\|q\|_M \quad \forall p,q\in M, \tag{12}$$

and the following inf-sup condition[24]

$$\sup_{\boldsymbol{v}\in U}\frac{b(q,\boldsymbol{v})}{\|\boldsymbol{v}\|_U}\geq\beta\|q\|_M, \tag{13}$$

where β is a positive constant.

Next, we give the semi discrete scheme of (8). Let $\{\Im_h\}$ be a uniformly regular family of triangulation or tetrahedron K of $\bar{\Omega}$, indexed by a parameter $h=\max_{K\in\Im_h}\{h_K;h_K=\mathrm{diam}(K)\}$. We introduce the mixed finite element subspaces $U_h\subset U$ and $M_h\subset M$. In addition, we set $X_h=U_h\times M_h$.

More important, we assume that (U_h,M_h) satisfies the following discrete inf-sup condition, i.e.,

$$\sup_{\boldsymbol{v}_h\in U_h}\frac{b\left(q_h,\boldsymbol{v}_h\right)}{\|\nabla\boldsymbol{v}_h\|_0}\geq\beta\left\|q_h\right\|_0 \quad \forall q_h\in M_h, \tag{14}$$

where β is a positive constant independent of h.

There are many finite spaces U_h and M_h that satisfy the discrete inf-sup conditions. We set P_k as the function space of polynomials of degree $\leq k$. For example, if we take finite element space $U_h\times M_h$ as Mini's element space [27], i.e.,

$$\begin{aligned}U_h&=\left\{\boldsymbol{v}_h\in U\cap C^0(\Omega)^d;\,\boldsymbol{v}_h|_K\in P_K \quad \forall K\in\Im_h\right\},\\ M_h&=\left\{q_h\in M\cap C^0(\Omega);\,q_h|_K\in P_1(K) \quad \forall K\in\Im_h\right\},\end{aligned}$$

where $P_K=P_1(K)^2\oplus\mathrm{span}\left\{\lambda_{K1}\lambda_{K2}\lambda_{K3}\right\}^2$ in two dimensions and $P_K=P_1(K)^3\oplus\mathrm{span}\left\{\lambda_{K1}\lambda_{K2}\lambda_{K3}\lambda_{K4}\right\}^3$ in three dimensions. In which λ_{Ki} are the barycentric coordinates corresponding to the vertex $A_i(i=1,2,3)$ of element K. For the definition of other stable MFE spaces, we refer to [24].

By the MFE spaces, we give the semi discrete scheme of (8): Find $\boldsymbol{u}_h\in H^2([0,T];U_h)$ and $p_h\in L^2([0,T];M_h)$.

$$\begin{cases}(\rho\dfrac{\partial^2\boldsymbol{u}_h}{\partial t^2},\boldsymbol{v}_h)+a(\boldsymbol{u}_h,\boldsymbol{v}_h)+b(p_h,\boldsymbol{v}_h)=(\boldsymbol{f},\boldsymbol{v}_h) \quad \forall\boldsymbol{v}_h\in U_h,\\ b(\boldsymbol{u}_h,q_h)-c(p_h,q_h)=0 \quad \forall q_h\in M_h,\\ (\boldsymbol{u}_h(0),\boldsymbol{v})=(\Pi_h^u\boldsymbol{u}_0,\boldsymbol{v}),\\ (\boldsymbol{u}_{ht}(0),\boldsymbol{v})=(\Pi_h^u\boldsymbol{u}_1,\boldsymbol{v}),\\ (p_h(0),q)=(\Pi_h^p p_0,q).\end{cases} \tag{15}$$

In the following analysis, we need to use the Stokes projection. Let $(\boldsymbol{u},p)$ be the solution of (8), then the discrete Stokes projection is defined as $(\Pi_h^u\boldsymbol{u},\Pi_h^p p)\in U_h\times M_h$ such that

$$a\left(\Pi_h^u\boldsymbol{u},\mathbf{v}_h\right)+b\left(\mathbf{v}_h,\Pi_h^p p\right)=a\left(\boldsymbol{u},\mathbf{v}_h\right)+b\left(\mathbf{v}_h,p\right) \quad \forall\mathbf{v}_h\in U_h, \tag{16}$$

$$b\left(\Pi_h^u\boldsymbol{u},q_h\right)=b\left(\boldsymbol{u},q_h\right) \quad \forall q_h\in M_h. \tag{17}$$

We have the following result of the Stokes projection by similar scaling argument of [26].

Lemma 3.2. *Let* $(\boldsymbol{u},p) \in (U \cap [H^{k+1}(\Omega)]^d) \times (M \cap H^k(\Omega))$ *satisfies* (8) *and* $(\Pi_h^u \boldsymbol{u}, \Pi_h^p p) \in U_h \times M_h$ *be the discrete Stokes projection defined above. Then the following estimate hold:*

$$\begin{aligned}
&\|\boldsymbol{u} - \Pi_h^u \boldsymbol{u}\|_0 + h\,|\boldsymbol{u} - \Pi_h^u \boldsymbol{u}|_1 \le Ch^{k+1}\left(|\boldsymbol{u}|_{k+1} + |p|_k\right),\\
&\|p - \Pi_h^p p\|_0 \le Ch^{k}\left(|\boldsymbol{u}|_{k+1} + |p|_k\right).
\end{aligned}$$

Before the proof begins, we set $v_t = \frac{\partial v}{\partial t}$ for any functions v. v_{tt}, v_{ttt} and v_{tttt} are similarly defined. The following theorem gives estimates for the L^2 norm of p and the H^1 norm of $\boldsymbol{u}$.

Theorem 3.3. *For* $t \ge 0$, *let* $(\boldsymbol{u},p)$ *be the solution of* (8) *and* $(\boldsymbol{u}_h, p_h)$ *be the solution of* (15). *Assume that* $\boldsymbol{u} \in L^\infty\left([H^{k+1}(\Omega)]^d\right), \boldsymbol{u}_t \in L^\infty\left([H^{k+1}(\Omega)]^d\right) \cap L^2\left([H^{k+1}(\Omega)]^d\right), \boldsymbol{u}_{tt} \in L^2\left([H^{k+1}(\Omega)]^d\right), p \in L^\infty\left(L^2(\Omega)\right)$, $p_t \in L^\infty\left(H^k(\Omega)\right) \cap L^2\left(H^k(\Omega)\right)$ *and* $p_{tt} \in L^2\left(H^k(\Omega)\right)$. *Then there are constants* C_1, C_2 *and* C_3 *independent on* h, *and* C_1 *is dependent on the* $\lambda^{-\frac{1}{2}}$ *such that*

$$\begin{aligned}
&\left\|\rho^{\frac{1}{2}}(\boldsymbol{u} - \boldsymbol{u}_h)_t\right\|_{L^\infty(L^2)} + \left\|\lambda^{-\frac{1}{2}}(p - p_h)\right\|_{L^\infty(L^2)} + \left\|(2\mu)^{\frac{1}{2}}\nabla(\boldsymbol{u} - \boldsymbol{u}_h)\right\|_{L^\infty(L^2)}\\
&\le C_1 h^k + C_2 h^k + C_3 h^{k+1}.
\end{aligned}$$

Proof. Using the previously defined Stokes projection (Π_h^u, Π_h^p) and a similar discussion process of Theorem 4.1 in [25], we can draw conclusions. □

To obtain the λ independent error estimate of pseudo-pressure, we give the following error estimate of $(\boldsymbol{u} - \boldsymbol{u}_h)_{tt}$.

Theorem 3.4. *For* $t \ge 0$, *let* $(\boldsymbol{u},p)$ *be the solution of* (8) *and* $(\boldsymbol{u}_h, p_h)$ *be the solution of* (15). *Assume that* $\boldsymbol{u}_t \in L^\infty\left([H^{k+1}(\Omega)]^d\right), \boldsymbol{u}_{tt} \in L^\infty\left([H^{k+1}(\Omega)]^d\right) \cap L^2\left([H^{k+1}(\Omega)]^d\right), \boldsymbol{u}_{ttt} \in L^2\left([H^{k+1}(\Omega)]^d\right), p_t \in L^\infty\left(L^2(\Omega)\right)$, $p_{tt} \in L^\infty\left(H^k(\Omega)\right) \cap L^2\left(H^k(\Omega)\right)$ *and* $p_{ttt} \in L^2\left(H^k(\Omega)\right)$. *Then there are constants* C_1,C_2 *and* C_3 *independent of* h, *and* C_1 *is dependent on the* $\lambda^{-\frac{1}{2}}$ *such that*

$$\left\|\rho^{\frac{1}{2}}(\boldsymbol{u} - \boldsymbol{u}_h)_{tt}\right\|_{L^\infty(L^2)} \le C_1 h^k + C_2 h^k + C_3 h^{k+1}.$$

Proof. Using the Stokes projection (Π_h^u, Π_h^p), we denote $\boldsymbol{\chi} = \boldsymbol{u}_h - \Pi_h^u \boldsymbol{u}$, $\boldsymbol{\eta} = \boldsymbol{u} - \Pi_h^u \boldsymbol{u}$, $\xi = p_h - \Pi_h^p p$ and $\zeta = p - \Pi_h^p p$. Then beginning with the error equation

$$\begin{aligned}
&(\rho\boldsymbol{\chi}_{tt}, \boldsymbol{v}_h) + a(\boldsymbol{\chi}, \boldsymbol{v}_h) + (\xi, \nabla\cdot\boldsymbol{v}_h)\\
&= (\rho\boldsymbol{\eta}_{tt}, \boldsymbol{v}_h) + a(\boldsymbol{\eta}, \boldsymbol{v}_h) + (\zeta, \nabla\cdot\boldsymbol{v}_h) \quad \forall \boldsymbol{v}_h \in \boldsymbol{U}_h, \qquad (18)\\
&\left(\lambda^{-1}\xi, q_h\right) - (\nabla\cdot\boldsymbol{\chi}, q_h) = \left(\lambda^{-1}\zeta, q_h\right) - (\nabla\cdot\boldsymbol{\eta}, q_h) \quad \forall q_h \in M_h, \qquad (19)
\end{aligned}$$

we differentiate (18) and (19) about t, then set $\boldsymbol{v}_h = \boldsymbol{\chi}_{tt}$ and add two formulations, we have

$$\begin{aligned}
&\frac{1}{2}\frac{d}{dt}\left\|\rho^{\frac{1}{2}}\boldsymbol{\chi}_{tt}\right\|^2_{L^2(\Omega)} + \frac{1}{2}\frac{d}{dt}\left\|\lambda^{-\frac{1}{2}}\xi_t\right\|^2_{L^2(\Omega)} + \frac{1}{2}\frac{d}{dt}\left\|(2\mu)^{\frac{1}{2}}\varepsilon(\boldsymbol{\chi_t})\right\|^2_{L^2(\Omega)}\\
&= (\rho\boldsymbol{\eta}_{ttt}, \boldsymbol{\chi}_{tt}) + \left(\lambda^{-1}\zeta_{tt}, \xi_t\right), \qquad (20)
\end{aligned}$$

where we use the property of Stokes projections Π_h^u and Π_h^p. By Cauchy-Schwarz's inequality and Young's inequality, we infer that

$$\begin{aligned}
&\frac{d}{dt}\left\|\rho^{\frac{1}{2}}\boldsymbol{\chi}_{tt}\right\|_{L^2(\Omega)}^2+\frac{d}{dt}\left\|\lambda^{-\frac{1}{2}}\xi_t\right\|_{L^2(\Omega)}^2+\frac{d}{dt}\left\|(2\mu)^{\frac{1}{2}}\varepsilon(\boldsymbol{\chi_t})\right\|_{L^2(\Omega)}^2\\
&\leq\left\|\rho^{\frac{1}{2}}\boldsymbol{\chi}_{tt}\right\|_{L^2(\Omega)}^2+\left\|\rho^{\frac{1}{2}}\boldsymbol{\eta}_{ttt}\right\|_{L^2(\Omega)}^2+\left\|\lambda^{-\frac{1}{2}}\zeta_{tt}\right\|_{L^2(\Omega)}^2+\left\|\lambda^{-\frac{1}{2}}\xi_t\right\|_{L^2(\Omega)}^2,
\end{aligned}\tag{21}$$

applying the Gronwall's inequality to (21) we obtain

$$\begin{aligned}
&\left\|\rho^{\frac{1}{2}}\boldsymbol{\chi}_{tt}\right\|_{L^2(\Omega)}^2(t)+\left\|\lambda^{-\frac{1}{2}}\xi_t\right\|_{L^2(\Omega)}^2(t)+\left\|(2\mu)^{\frac{1}{2}}\varepsilon(\boldsymbol{\chi_t})\right\|_{L^2(\Omega)}^2(t)\\
&\leq\left\|\rho^{\frac{1}{2}}\boldsymbol{\chi}_{tt}(0)\right\|_{L^2(\Omega)}^2+\left\|\lambda^{-\frac{1}{2}}\xi_t(0)\right\|_{L^2(\Omega)}+\left\|(2\mu)^{\frac{1}{2}}\varepsilon(\boldsymbol{\chi_t}(0))\right\|_{L^2(\Omega)}^2\\
&+\int_0^t\left(\left\|\rho^{\frac{1}{2}}\boldsymbol{\eta}_{ttt}\right\|_{L^2(\Omega)}^2+\left\|\lambda^{-\frac{1}{2}}\zeta_{tt}\right\|_{L^2(\Omega)}^2\right).
\end{aligned}\tag{22}$$

We take the maximum over all t and choose appropriate initial conditions such that $\varepsilon(\boldsymbol{\chi_t}(0))=\boldsymbol{\chi}_{tt}(0)=\xi_t(0)=0$, then we have

$$\begin{aligned}
&\left\|\rho^{\frac{1}{2}}\boldsymbol{\chi}_{tt}\right\|_{L^\infty(L^2)}^2+\left\|\lambda^{-\frac{1}{2}}\xi_t\right\|_{L^\infty(L^2)}^2+\left\|(2\mu)^{\frac{1}{2}}\varepsilon(\boldsymbol{\chi_t})\right\|_{L^\infty(L^2)}^2\\
&\leq\left\|\rho^{\frac{1}{2}}\boldsymbol{\eta}_{ttt}\right\|_{L^2(L^2)}^2+\left\|\lambda^{-\frac{1}{2}}\zeta_{tt}\right\|_{L^2(L^2)}^2,
\end{aligned}\tag{23}$$

By the triangle inequality and the Lemma 3.2, we complete the proof. □

Further, we can also estimate the L^2 error of $\boldsymbol{u}$.

Theorem 3.5. *For $t\geq 0$, let $(\boldsymbol{u},p)$ be the solution of (8) and $(\boldsymbol{u}_h,p_h)$ be the solution of (15). Assume $\boldsymbol{u}\in L^\infty\left([H^{k+1}(\Omega)]^d\right)\cap L^2\left([H^{k+1}(\Omega)]^d\right),\boldsymbol{u}_t\in L^2\left([H^{k+1}(\Omega)]^d\right),p\in L^\infty\left(H^k(\Omega)\right)\cap L^2\left(H^k(\Omega)\right)$ and $p_t\in L^2\left(H^k(\Omega)\right)$. Then there are constants C_1 and C_2 independent on h, and C_1 is dependent on the $\lambda^{-\frac{1}{2}}$ such that*

$$\left\|\rho^{\frac{1}{2}}(\boldsymbol{u}-\boldsymbol{u}_h)\right\|_{L^\infty(L^2)}\leq C_1h^k+C_2h^{k+1}.$$

Proof. Using the similar argument of Theorem 4.2 in [25], we can complete the proof. □

Remark 3.1. *From Theorem 3.3 and Theorem 3.5, we note the MFE for the elastic wave equation is locking-free when $\lambda\to\infty$.*

Next, we give the error estimate of $\|p-p_h\|$ independent on $\lambda^{-\frac{1}{2}}$ by inf-sup condition.

Theorem 3.6. *Under the same assumptions of Theorem 3.3 and Theorem 3.4. There exists a positive constant C depending on regularity of $\boldsymbol{u},\boldsymbol{u}_t,\boldsymbol{u}_{tt},\boldsymbol{u}_{ttt},p,p_t,p_{tt},p_{ttt}$ such that the following estimate holds:*

$$\|p-p_h\|_{L^\infty(L^2)}\leq Ch^k.$$

Proof. Let $q_h \in M_h$ be an arbitrary element. We can conclude the following result from the discrete inf-sup condition:

$$\begin{aligned}\beta \left\| p_h(t) - q_h \right\| &\leq \sup_{\substack{\boldsymbol{v}_h \in U_h \\ \boldsymbol{v}_h \neq 0}} \frac{b\left(\boldsymbol{v}_h, p_h - q_h\right)}{\left\|\boldsymbol{v}_h\right\|_1} \\ &= \sup_{\substack{\boldsymbol{v}_h \in U_h \\ \boldsymbol{v}_h \neq 0}} \frac{b\left(\boldsymbol{v}_h, p_h - p\right) + b\left(\boldsymbol{v}_h, p - q_h\right)}{\left\|\boldsymbol{v}_h\right\|_1}, \end{aligned} \tag{24}$$

where β is a constant.

Replacing $\boldsymbol{v}$ by $\boldsymbol{v}_h$ in (8) and subtracting (8) from (15), we have

$$b\left(\boldsymbol{v}_h, p - p_h\right) = \underbrace{\left(\rho(\boldsymbol{u}_h)_{tt}, \boldsymbol{v}_h\right) - \left(\rho \boldsymbol{u}_{tt}, \boldsymbol{v}_h\right)}_{=:H_1} + \underbrace{a\left(\boldsymbol{u}_h, \boldsymbol{v}_h\right) - a\left(\boldsymbol{u}, \boldsymbol{v}_h\right)}_{=:H_2},$$

then we split the right term into two parts H_1 and H_2. Exploiting Cauchy-Schwarz inequality, we estimate that

$$\left|H_1\right| \leq C \left\|\left(\boldsymbol{u}_h\right)_{tt} - \boldsymbol{u}_{tt}\right\| \left\|\boldsymbol{v}_h\right\|, \quad \left|H_2\right| \leq C \left(\left|\boldsymbol{u}_h - \boldsymbol{u}\right|_1\right) \left|\boldsymbol{v}_h\right|_1,$$

From Theorem 3.4 and Theorem 3.3. We deduce that

$$\frac{b\left(\boldsymbol{v}_h, p - p_h\right)}{\left\|\boldsymbol{v}_h\right\|_1} \leq (C_1 h^k + C_2 h^k + C_3 h^{k+1})h + (C_1^\star h^k + C_2^\star h^k + C_3^\star h^{k+1}), \tag{25}$$

where C_1, C_2, C_3 are constants given in Theorem 3.4 and $C_1^\star$, $C_2^\star$, $C_3^\star$ are constants given in Theorem 3.3. Then we get

$$\frac{b\left(\boldsymbol{v}_h, p - p_h\right)}{\left\|\boldsymbol{v}_h\right\|_1} \leq C h^k, \tag{26}$$

where C is positive generic constant that depends on the regularity of $\mathbf{u}$, $\mathbf{u}_t$, $\mathbf{u}_{tt}$, $\mathbf{u}_{ttt}$, p, p_t, p_{tt}, p_{ttt}. Then substituting (26) into (24), we obtain

$$\beta \left\| p_h - q_h \right\| \leq C h^k + \left\| p - q_h \right\|,$$

by triangle inequality, we have

$$\left\| p - p_h \right\| \leq C(\left\| p - q_h \right\| + \left\| p_h - q_h \right\|) \leq C \left(h^k + \left\| p - q_h \right\|\right), \tag{27}$$

where q_h is an arbitrary element of M_h. Hence, the equation (27) becomes

$$\left\| p - p_h \right\| \leq C h^k + \inf_{q_h \in M_h} \left\| p - q_h \right\|, \tag{28}$$

Choosing $q_h = \Pi_h^p p$, using Lemma 3.2, and taking the maximum on the left. We have the desired result of Theorem 3.6. □

3.3. Fully discrete scheme. In this section, we present the theoretical analysis of the fully discrete scheme of (15). Let N be the number of time divisions in the time domain, $\Delta t = T/N$ denotes the time step, and $t_i = i\Delta t, i = 1, \cdots N$. For any function g of time, let g^n denotes $g(t_n)$. For convenience, we define the following operator:

$$\begin{aligned} &g^{n+\frac{1}{2}} = \frac{\left(g^{n+1} + g^n\right)}{2}, \partial_t g^{n+\frac{1}{2}} = \frac{g^{n+1} - g^n}{\Delta t}, g^{n,\frac{1}{2}} = \frac{\left(g^{n+1} + g^{n-1}\right)}{2}, \\ &\partial_t^2 g^n = \frac{\partial_t g^{n+\frac{1}{2}} - \partial_t g^{n-\frac{1}{2}}}{\Delta t} = \frac{g^{n+1} - 2g^n + g^{n-1}}{\Delta t^2}, \\ &\partial_t g^n = \frac{\partial_t g^{n+\frac{1}{2}} + \partial_t g^{n-\frac{1}{2}}}{2} = \frac{g^{n+1} - g^{n-1}}{2\Delta t}. \end{aligned}$$

By using these operators, the implicit fully discrete scheme below can be obtained. Find $\boldsymbol{u}_h^{n+1}$ and p_h^{n+1} such that

$$\left(\rho\partial_t^2\boldsymbol{u}_h^n,\boldsymbol{v}_h\right)+a\left(\boldsymbol{u}_h^{n,\frac{1}{2}},\boldsymbol{v}_h\right)+b\left(p_h^{n,\frac{1}{2}},\boldsymbol{v}_h\right)=\left(\boldsymbol{f}^{n,\frac{1}{2}},\boldsymbol{v}_h\right),\forall\boldsymbol{v}_h\in U_h, \tag{29}$$

$$b\left(\boldsymbol{u}_h^{n+\frac{1}{2}},q_h\right)-c\left(p_h^{n+\frac{1}{2}},q_h\right)=0,\forall q_h\in M_h, \tag{30}$$

$$\begin{aligned}&\left(\rho\partial_t\boldsymbol{u}_h^{\frac{1}{2}},\boldsymbol{v}_h\right)+\frac{\Delta t^2}{2}a\left(\partial_t\boldsymbol{u}_h^{\frac{1}{2}},\boldsymbol{v}_h\right)+\frac{\Delta t}{2}a\left(\boldsymbol{u}_h^0,\boldsymbol{v}_h\right)\\&+\frac{\Delta t^2}{2}b\left(\boldsymbol{v}_h,\partial_t p_h^{\frac{1}{2}}\right)+\frac{\Delta t}{2}b\left(\boldsymbol{v}_h,p_h^0\right)\\&=\frac{\Delta t^2}{2}\left(\partial_t\boldsymbol{f}^{\frac{1}{2}},\boldsymbol{v}_h\right)+\frac{\Delta t}{2}\left(\partial_t\boldsymbol{f}^0,\boldsymbol{v}_h\right)+\left(\rho\Pi_h^u\boldsymbol{u}_1,\boldsymbol{v}_h\right),\end{aligned} \tag{31}$$

$$\left(\boldsymbol{u}^0,\boldsymbol{v}_h\right)=\left(\Pi_h^u\boldsymbol{u}_0,\boldsymbol{v}_h\right), \tag{32}$$

$$\left(p_h^0,q_h\right)=\left(\Pi_h^p p_0,q_h\right), \tag{33}$$

where (31) is used to compute $\mathbf{u}_h^1$. Note that the fully discrete scheme is an implicit method. Then by the similar argument of the explicit method in Theorem 5.1 of [25], we know the fully discrete scheme is unconditionally stable. Here we only give the error estimate for brevity.

Theorem 3.7. *Under the assumption of Theorem 3.3 and Theorem 3.6, if* $\boldsymbol{u}\in L^\infty([H^{k+1}(\Omega)]^d),\boldsymbol{u}_{ttt}\in L^\infty\left([\boldsymbol{L}^2(\Omega)]^d\right)$, $p_{ttt}\in L^\infty\left(\boldsymbol{L}^2(\Omega)\right),\boldsymbol{u}_{tttt}\in L^\infty\left([\boldsymbol{L}^2(\Omega)]^d\right)$, $p\in L^\infty\left(H^k(\Omega)\right)$*, then for* $(\boldsymbol{u}_h(t),p_h(t))$ *defined by* (29)-(33)*, there exists a constant* C *independent on* h *and* Δt*, and dependent on regularity of solution such that*

$$\begin{aligned}&\|\rho^{\frac{1}{2}}(\boldsymbol{u}(t_n)-\boldsymbol{u}_h^n)\|_{l^\infty(L^2)}+\|(p(t_n)-p_h^n)\|_{l^\infty(L^2)}\\&+\|\nabla(\boldsymbol{u}(t_n)-\boldsymbol{u}_h^n)\|_{l^\infty(L^2)}\le C\left(h^k+\Delta t^2\right).\end{aligned}$$

Proof. Subtracting (29)-(30) from (8), combing with the properties of the Π_h^u and Π_h^p we have:

$$\left(\rho\partial_t^2\boldsymbol{\chi}^n,\boldsymbol{v}_h\right)+a\left(\boldsymbol{\chi}^{n,\frac{1}{2}},\boldsymbol{v}_h\right)+b\left(\xi^{n,\frac{1}{2}},\boldsymbol{v}_h\right)=\left(\rho\partial_t^2\boldsymbol{\eta}^n,\boldsymbol{v}_h\right)+\left(\boldsymbol{r}^n,\boldsymbol{v}_h\right), \tag{34}$$

$$\left(\lambda^{-1}\xi^{n+\frac{1}{2}},q_h\right)-b\left(q_h,\boldsymbol{\chi}^{n+\frac{1}{2}}\right)=\left(\lambda^{-1}\zeta^{n+\frac{1}{2}},q_h\right), \tag{35}$$

where $\boldsymbol{r}^n=\rho\left(\boldsymbol{u}_{tt}^{n,1/2}-\partial_t^2\boldsymbol{u}^n\right)$. The $\boldsymbol{\chi}$, $\boldsymbol{\eta}$, ξ and ζ are same with the proof of Theorem 3.4

We introduce some new variables here:

$$\phi^n=\Delta t\sum_{i=0}^{n-1}\xi^{i+\frac{1}{2}},\quad\phi^0=0,\quad\psi^n=\Delta t\sum_{i=0}^{n-1}\boldsymbol{\chi}^{i+\frac{1}{2}},\quad\psi^0=0,$$

noting that

$$\phi^{n+\frac{1}{2}}=\frac{\Delta t}{2}\xi^{\frac{1}{2}}+\frac{\Delta t}{2}\sum_{i=1}^{n}(\xi^{i+\frac{1}{2}}+\xi^{i-\frac{1}{2}}),\quad\psi^{n+\frac{1}{2}}=\frac{\Delta t}{2}\boldsymbol{\chi}^{\frac{1}{2}}+\frac{\Delta t}{2}\sum_{i=1}^{n}(\boldsymbol{\chi}^{i+\frac{1}{2}}+\boldsymbol{\chi}^{i-\frac{1}{2}}).$$

Then we consider (8) at $n=0$ and $n=1$, and use the Taylor expansion. We infer

$$\begin{aligned}&(\rho\partial_t(\boldsymbol{u}_{tt}^{\frac{1}{2}}),\boldsymbol{v}_h)+a(\partial_t\boldsymbol{u}^{\frac{1}{2}},\boldsymbol{v}_h)+b(\partial_t p^{\frac{1}{2}},\boldsymbol{v}_h)=(\partial_t\boldsymbol{f}^{\frac{1}{2}},\boldsymbol{v}_h),\\&\partial_t\boldsymbol{u}^{\frac{1}{2}}=\boldsymbol{u}_t(0)+\frac{\Delta t}{2}\boldsymbol{u}_{tt}^0+\frac{1}{2\Delta t}\int_0^{\Delta t}(\Delta t-t)^2\frac{\partial^3\boldsymbol{u}}{\partial t^3}(t)dt.\end{aligned}$$

Hence,

$$
\begin{aligned}
&(\rho\partial_t \boldsymbol{u}^{\frac{1}{2}}, \boldsymbol{v}_h) + \frac{\Delta t^2}{2} a(\partial_t \boldsymbol{u}^{\frac{1}{2}}, \boldsymbol{v}_h) + \frac{\Delta t^2}{2} b(\partial_t p^{\frac{1}{2}}, \boldsymbol{v}_h) \\
&= (\rho \boldsymbol{u}_t(0), \boldsymbol{v}_h) + \frac{\Delta t \rho}{2} (\boldsymbol{u}_{tt}^0, \boldsymbol{v}_h) + \frac{1}{2\Delta t} \int_0^{\Delta t} (\Delta t - t)^2 (\rho \frac{\partial^3 \boldsymbol{u}}{\partial t^3}, \boldsymbol{v}_h) dt \\
&+ \frac{\Delta t^2}{2} (\partial_t \boldsymbol{f}^{\frac{1}{2}}, \boldsymbol{v}_h) - \frac{\Delta t^2}{2} (\rho \partial_t (\boldsymbol{u}_{tt}^{\frac{1}{2}}), \boldsymbol{v}_h).
\end{aligned}
$$

Subtracting the above equation form (31), considering the initial condition and the consistency we have

$$
\begin{aligned}
&(\rho\partial_t \boldsymbol{\chi}^{\frac{1}{2}}, \boldsymbol{v}_h) + \frac{\Delta t^2}{2} a(\partial_t \boldsymbol{\chi}^{\frac{1}{2}}, \boldsymbol{v}_h) + \frac{\Delta t}{2} a(\boldsymbol{\chi}^0, \boldsymbol{v}_h) \\
&+ \frac{\Delta t^2}{2} b(\partial_t \xi^{\frac{1}{2}}, \boldsymbol{v}_h) + \frac{\Delta t}{2} b(\xi^0, \boldsymbol{v}_h) \\
&= (\rho\partial_t \boldsymbol{\eta}^{\frac{1}{2}}, \boldsymbol{v}_h) + (\rho(\Pi_h^u \boldsymbol{u}_1 - \boldsymbol{u}_1), \boldsymbol{v}_h) \\
&- \frac{1}{2\Delta t} \int_0^{\Delta t} (\Delta t - t)^2 (\rho \frac{\partial^3 \boldsymbol{u}}{\partial t^3}, \boldsymbol{v}_h) dt + \frac{\Delta t^2}{2} (\rho \partial_t (\boldsymbol{u}_{tt}^{\frac{1}{2}}), \boldsymbol{v}_h). \qquad (36)
\end{aligned}
$$

(34) can be rewritten as

$$
\begin{aligned}
&(\rho\partial_t^2 \boldsymbol{\chi}^n, \boldsymbol{v}_h) + \frac{1}{2} a(\boldsymbol{\chi}^{n+\frac{1}{2}} + \boldsymbol{\chi}^{n-\frac{1}{2}}, \boldsymbol{v}_h) + \frac{\Delta t^2}{4} a(\partial_t^2 \boldsymbol{\chi}^n, \boldsymbol{v}_h) \\
&+ \frac{1}{2} b(\xi^{n+\frac{1}{2}} + \xi^{n-\frac{1}{2}}, \boldsymbol{v}_h) + \frac{\Delta t^2}{4} b(\partial_t^2 \xi^n, \boldsymbol{v}_h) \\
&= (\rho\partial_t^2 \boldsymbol{\eta}^n, \boldsymbol{v}_h) + (\Delta t \sum_{i=1}^n \boldsymbol{r}^i, \boldsymbol{v}_h), n \geq 1. \qquad (37)
\end{aligned}
$$

Then summing over all time intervals of (37), we have

$$
\begin{aligned}
&(\rho\partial_t \boldsymbol{\chi}^{n+\frac{1}{2}} - \rho\partial_t \boldsymbol{\chi}^{\frac{1}{2}}, \boldsymbol{v}_h) + \frac{\Delta t}{2} \sum_{i=1}^n a(\boldsymbol{\chi}^{i+\frac{1}{2}} + \boldsymbol{\chi}^{i-\frac{1}{2}}, \boldsymbol{v}_h) \\
&+ \frac{\Delta t^2}{4} a(\partial_t \boldsymbol{\chi}^{n+\frac{1}{2}} - \partial_t \boldsymbol{\chi}^{\frac{1}{2}}, \boldsymbol{v}_h) \\
&+ \frac{\Delta t}{2} \sum_{i=1}^n b(\xi^{i+\frac{1}{2}} + \xi^{i-\frac{1}{2}}, \boldsymbol{v}_h) + \frac{\Delta t^2}{4} b(\partial_t \xi^{n+\frac{1}{2}} - \partial_t \xi^{\frac{1}{2}}, \boldsymbol{v}_h) \\
&= (\rho\partial_t \boldsymbol{\eta}^{n+\frac{1}{2}} - \rho\partial_t \boldsymbol{\eta}^{\frac{1}{2}}, \boldsymbol{v}_h) + (\Delta t \sum_{i=1}^n \boldsymbol{r}^i, \boldsymbol{v}_h). \qquad (38)
\end{aligned}
$$

Taking (36) into (38), using the initial condition $\boldsymbol{\chi}^0 = 0$ and $\xi^0 = 0$, noting $\partial_t \boldsymbol{\chi}^{\frac{1}{2}} = \frac{2}{\Delta t} \boldsymbol{\chi}^{\frac{1}{2}}$ and $\partial_t \xi^{\frac{1}{2}} = \frac{2}{\Delta t} \xi^{\frac{1}{2}}$, combining with the definition of ϕ and ψ, we infer that

$$
\begin{aligned}
&(\rho\partial_t \boldsymbol{\chi}^{n+\frac{1}{2}}, \boldsymbol{v}_h) + \frac{\Delta t^2}{4} a(\partial_t \boldsymbol{\chi}^{n+\frac{1}{2}}, \boldsymbol{v}_h) + a(\psi^{n+\frac{1}{2}}, \boldsymbol{v}_h) \\
&+ \frac{\Delta t^2}{4} b(\partial_t \xi^{n+\frac{1}{2}}, \boldsymbol{v}_h) + b(\phi^{n+\frac{1}{2}}, \boldsymbol{v}_h) \\
&= (\rho\partial_t \boldsymbol{\eta}^{n+\frac{1}{2}}, \boldsymbol{v}_h) + (\boldsymbol{R}^n, \boldsymbol{v}_h), \qquad (39)
\end{aligned}
$$

where $\boldsymbol{R}^n$ is defined as

$$\boldsymbol{R}^n = \Delta t \sum_{i=1}^{n} \boldsymbol{r}^i + \rho\left(\Pi_h^u \boldsymbol{u}_1 - \boldsymbol{u}_1\right) - \frac{1}{2\Delta t}\int_0^{\Delta t} \rho(\Delta t - t)^2 \frac{\partial^3 \boldsymbol{u}}{\partial t^3}(t)dt + \frac{1}{2}\Delta t^2 \rho \partial_t(\boldsymbol{u}_{tt}^{\frac{1}{2}}).$$

In addition, we set $\boldsymbol{v}_h = \boldsymbol{\chi}^{n+\frac{1}{2}}$ in (39) and $q_h = \phi^{n+\frac{1}{2}}$ in (35), note that $\partial_t \phi^{n+\frac{1}{2}} = \xi^{n+\frac{1}{2}}$ and $\partial_t \psi^{n+\frac{1}{2}} = \boldsymbol{\chi}^{n+\frac{1}{2}}$, adding (39) and (35) we have

$$\begin{aligned}
&(\rho \partial_t \boldsymbol{\chi}^{n+\frac{1}{2}}, \boldsymbol{\chi}^{n+\frac{1}{2}}) + \frac{\Delta t^2}{4} a(\partial_t \boldsymbol{\chi}^{n+\frac{1}{2}}, \boldsymbol{\chi}^{n+\frac{1}{2}}) + a(\psi^{n+\frac{1}{2}}, \partial_t \psi^{n+\frac{1}{2}}) \\
&+ \frac{\Delta t^2}{4} b(\partial_t \xi^{n+\frac{1}{2}}, \boldsymbol{\chi}^{n+\frac{1}{2}}) + (\lambda^{-1} \partial_t \phi^{n+\frac{1}{2}}, \phi^{n+\frac{1}{2}}) \\
&= (\rho \partial_t \boldsymbol{\eta}^{n+\frac{1}{2}}, \boldsymbol{\chi}^{n+\frac{1}{2}}) + (\boldsymbol{R}^n, \boldsymbol{\chi}^{n+\frac{1}{2}}) + (\lambda^{-1}\zeta^{n+\frac{1}{2}}, \phi^{n+\frac{1}{2}}). \qquad (40)
\end{aligned}$$

We take $q_h = \partial_t \xi^{n+\frac{1}{2}}$ in (35), note that the term $b(\partial_t \xi^{n+\frac{1}{2}}, \boldsymbol{\chi}^{n+\frac{1}{2}})$ has the following form

$$b(\partial_t \xi^{n+\frac{1}{2}}, \boldsymbol{\chi}^{n+\frac{1}{2}}) = (\lambda^{-1}\xi^{n+\frac{1}{2}}, \partial_t \xi^{n+\frac{1}{2}}) - (\lambda^{-1}\zeta^{n+\frac{1}{2}}, \partial_t \xi^{n+\frac{1}{2}}).$$

Take the formula into (40) we obtain

$$\begin{aligned}
&(\rho \partial_t \boldsymbol{\chi}^{n+\frac{1}{2}}, \boldsymbol{\chi}^{n+\frac{1}{2}}) + \frac{\Delta t^2}{4} a(\partial_t \boldsymbol{\chi}^{n+\frac{1}{2}}, \boldsymbol{\chi}^{n+\frac{1}{2}}) + a(\psi^{n+\frac{1}{2}}, \partial_t \psi^{n+\frac{1}{2}}) \\
&+ \frac{\Delta t^2}{4} (\lambda^{-1} \xi^{n+\frac{1}{2}}, \partial_t \xi^{n+\frac{1}{2}}) + (\lambda^{-1} \partial_t \phi^{n+\frac{1}{2}}, \phi^{n+\frac{1}{2}}) \\
&= (\rho \partial_t \boldsymbol{\eta}^{n+\frac{1}{2}}, \boldsymbol{\chi}^{n+\frac{1}{2}}) + (\boldsymbol{R}^n, \boldsymbol{\chi}^{n+\frac{1}{2}}) \\
&+ \frac{\Delta t^2}{4} (\lambda^{-1}\zeta^{n+\frac{1}{2}}, \phi^{n+\frac{1}{2}}) + (\lambda^{-1}\zeta^{n+\frac{1}{2}}, \partial_t \xi^{n+\frac{1}{2}}). \qquad (41)
\end{aligned}$$

Summing (41) over all the time intervals and multiplying $2\Delta t$ on the both side, using the Cauchy-Schwarz's inequality, we have

$$\begin{aligned}
&\|\rho^{\frac{1}{2}} \boldsymbol{\chi}^{n+\frac{1}{2}}\|_{L^2}^2 - \|\rho^{\frac{1}{2}} \boldsymbol{\chi}^0\|_{L^2}^2 + \frac{\Delta t^2}{4}(\|\nabla \boldsymbol{\chi}^{n+1}\|_{L^2}^2 - \|\nabla \boldsymbol{\chi}^0\|_{L^2}^2) + \|\nabla \psi^{n+1}\|_{L^2}^2 - \|\nabla \psi^0\|_{L^2}^2 \\
&+ \frac{\Delta t^2}{4}\|(\lambda^{-\frac{1}{2}}\xi^{n+1}\|_{L^2}^2 - \|\lambda^{-\frac{1}{2}}\xi^0\|_{L^2}^2) + \|\lambda^{-\frac{1}{2}}\phi^{n+1}\|_{L^2}^2 - \|\lambda^{-\frac{1}{2}}\phi^0\|_{L^2}^2 \\
&\leq \frac{1}{2}\Delta t^2 \sum_{i=0}^{n} \|\lambda^{-\frac{1}{2}}\zeta^{i+\frac{1}{2}}\|_{L^2}(\|\lambda^{-\frac{1}{2}}\xi^{i+1}\|_{L^2} + \|\lambda^{-\frac{1}{2}}\xi^i\|_{L^2}) \\
&+ 2\Delta t \sum_{i=0}^{n} \|\boldsymbol{\chi}^{i+\frac{1}{2}}\|_{L^2}(\|\rho \partial_t \boldsymbol{\eta}^{i+\frac{1}{2}}\|_{L^2} + \|\boldsymbol{R}^i\|_{L^2}) + 2\Delta t \sum_{i=0}^{n} \|\lambda^{-\frac{1}{2}}\zeta^{i+\frac{1}{2}}\|_{L^2}\|\lambda^{-\frac{1}{2}}\phi^{i+\frac{1}{2}}\|_{L^2}.
\end{aligned}$$

By the inequality $\|\lambda^{-\frac{1}{2}}\xi^i\|_{L^2} \leq \|\lambda^{-\frac{1}{2}}\xi\|_{l^\infty(L^2)}$ and $\|\lambda^{-\frac{1}{2}}\boldsymbol{\chi}^i\|_{L^2} \leq \|\lambda^{-\frac{1}{2}}\boldsymbol{\chi}\|_{l^\infty(L^2)}$, using the initial condition, taking the maximum over time on the left side, noting $N\Delta t = T$ we infer

$$\begin{aligned}
&\|\rho^{\frac{1}{2}}\boldsymbol{\chi}\|_{l^\infty(L^2)}^2 + \|\lambda^{-\frac{1}{2}}\phi\|_{l^\infty(L^2)}^2 + \|\lambda^{-\frac{1}{2}}\psi\|_{l^\infty(H^1)}^2 \\
&\leq C\left(\|\lambda^{-\frac{1}{2}}\zeta\|_{l^\infty(L^2)}^2 + \Delta t^2(\sum_{i=0}^{N-1}\|\rho \partial_t \boldsymbol{\eta}^{i+\frac{1}{2}}\|_{L^2}^2) + \Delta t^2(\sum_{i=0}^{N-1}\|\boldsymbol{R}^i\|_{L^2})^2\right). \qquad (42)
\end{aligned}$$

After applying the similar proof as in Theorem 5.2 in [28], we can derive an estimate for the second term on the right-hand side of (42) combined with the Lemma 3.2

$$\Delta t \sum_{i=0}^{N-1} \|\rho \partial_t \boldsymbol{\eta}^{i+\frac{1}{2}}\|_{L^2} \leq C(h^2 \|\boldsymbol{u}\|_{L^\infty(H^2)} + h^2 \|p\|_{L^\infty(H^1)} + \Delta t^2 \|\boldsymbol{u}_{ttt}\|_{L^1(L^2)} + \Delta t^2 \|p_{ttt}\|_{L^1(L^2)}),$$

For the third term, we can use the similar proof of Theorem 5.2 in [28] by Taylor expansion

$$\Delta t \sum_{i=0}^{N-1} \|\boldsymbol{R}^i\|_{L^2} \leq C(h^2 + \Delta t^2),$$

where C depends on the regularity of $\|\boldsymbol{u}_{tttt}\|_{L^1(L^2)}$ in the above inequality. For the first term $\|\lambda^{-\frac{1}{2}}\zeta\|_{l^\infty(L^2)}$, we can use the Lemma 3.2 to bound it. Hence, we give the following result for (42) combined with the triangle inequality:

$$\begin{aligned} &\|\rho^{\frac{1}{2}}(\boldsymbol{u}(t^n) - \boldsymbol{u}_h^n)\|_{l^\infty(L^2)} + \|\lambda^{-\frac{1}{2}}(p(t^n) - p_h^n)\|_{l^\infty(L^2)} \\ &+ \|\nabla(\boldsymbol{u}(t^n) - \boldsymbol{u}_h^n)\|_{l^\infty(L^2)} \\ &\leq Ch(\|\boldsymbol{u}\|_{L^\infty(H^2)} + \|p\|_{L^\infty(H^1)}) \\ &+ C\Delta t^2(\|\boldsymbol{u}_{ttt}\|_{L^1(L^2)} + \|p_{ttt}\|_{L^1(L^2)}). \end{aligned} \tag{43}$$

We need to obtain the λ independent error estimate of p by the inf-sup condition. First we rewrite (34) into the following form:

$$(\xi^{n,\frac{1}{2}}, \nabla \cdot \boldsymbol{v}_h) = -(\rho \partial_t^2 \boldsymbol{\chi}^n, \boldsymbol{v}_h) - a(\boldsymbol{\chi}^{n,\frac{1}{2}}, \boldsymbol{v}_h) + (\rho \partial_t^2 \boldsymbol{\eta}^n, \boldsymbol{v}_h) + (\boldsymbol{r}^n, \boldsymbol{v}_h).$$

Then using the bound of (42)-(43), the inverse inequality and the continuity of bilinear a, we derive that

$$\begin{aligned} &|-(\rho \partial_t^2 \boldsymbol{\chi}^n, \boldsymbol{v}_h) - a(\boldsymbol{\chi}^{n,\frac{1}{2}}, \boldsymbol{v}_h) + (\rho \partial_t^2 \boldsymbol{\eta}^n, \boldsymbol{v}_h)| \\ &\leq C(h + \Delta t^2)h\|\boldsymbol{v}_h\|_{H^1} + C(h + \Delta t^2)\|\boldsymbol{v}_h\|_{H^1} \leq C(h + \Delta t^2)\|\boldsymbol{v}_h\|_{H^1}. \end{aligned}$$

Next, we will obtain the following result by Taylor expansion

$$|(\boldsymbol{r}^n, \boldsymbol{v}_h)| \leq C\Delta t^2 \|\boldsymbol{u}_{tttt}\|_{L^\infty(L^2)} \|\boldsymbol{v}\|.$$

Using the inf-sup condition we infer

$$\begin{aligned} \beta\|\xi^{n,\frac{1}{2}}\| &\leq \sup_{\boldsymbol{v}_h \in H^1, \boldsymbol{v}_h \neq 0} \frac{|-(\rho \partial_t^2 \boldsymbol{\chi}^n, \boldsymbol{v}_h) - a(\boldsymbol{\chi}^{n,\frac{1}{2}}, \boldsymbol{v}_h) + (\rho \partial_t^2 \boldsymbol{\eta}^n, \boldsymbol{v}_h) + (\boldsymbol{r}^n, \boldsymbol{v}_h)|}{\|\boldsymbol{v}_h\|_{H^1}} \\ &\leq C(h + \Delta t^2). \end{aligned}$$

Then taking the maximum on the left side, there exists a constant C independent on h and Δt such that

$$\|\xi\|_{l^\infty(L^2)} \leq C(h + \Delta t^2).$$

Combining with the triangle inequality and the approximation property of $\|\zeta\|_{l^\infty(L^2)}$ we complete the proof. □

4. The POD-ROM

In this section, we are going to give a reduced-order model using POD technique.

4.1. The POD method. The POD method mainly provides a useful tool for efficiently approximating a large amount of data. The method essentially provides an orthogonal basis for representing the given data in a certain least squares optimal sense.

For solutions $\boldsymbol{U}_i(x,y) = \left((u_x^{n_i})_h, (u_y^{n_i})_h, p_h^{n_i}\right)^T (i = 1, 2, \ldots, L)$ obtained from (29)-(33), we set

$$\mathcal{W} = \operatorname{span}\{\boldsymbol{U}_1, \boldsymbol{U}_2, \ldots, \boldsymbol{U}_L\},$$

as the ensemble of the snapshots $\{\boldsymbol{U}_i\}_{i=1}^L$. Let $\{\boldsymbol{\psi}_j\}_{j=1}^l$ denote an orthonormal basis of $\mathcal{W}$ with $l = \dim \mathcal{W}$. Then each member of $\mathcal{W}$ can be defined as

$$\boldsymbol{U}_i = \sum_{j=1}^{l} \left(\boldsymbol{U}_i, \boldsymbol{\psi}_j\right)_{X_h} \psi_j \text{ for } i = 1, 2, \ldots, L, \tag{44}$$

where $\left(\boldsymbol{U}_i, \boldsymbol{\psi}_j\right)_{X_h} \boldsymbol{\psi}_j = \left(\left(\nabla \boldsymbol{u}_h^{n_i}, \nabla \boldsymbol{\psi}_{uj}\right)_0 \boldsymbol{\psi}_{uj}, \left(p_h^{n_i}, \psi_{pj}\right)_0 \psi_{pj}\right)$, and $(\cdot,\cdot)_0$ denotes L^2-inner product, $\boldsymbol{\psi}_{uj}$ and ψ_{pj} are orthonormal basis corresponding to $\boldsymbol{u}$ and p, respectively.

Definition 4.1 (POD method[17])**.** *The method of POD consists in finding the orthonormal basis such that for every $d(1 \le d \le l)$ the mean square error between the elements $\boldsymbol{U}_i$ $(1 \le i \le L)$ and the corresponding d-th partial sum of* (44) *is minimized on average:*

$$\min_{\{\boldsymbol{\psi}_j\}_{j=1}^d} \frac{1}{L} \sum_{i=1}^{L} \left\| \boldsymbol{U}_i - \sum_{j=1}^{d} \left(\boldsymbol{U}_i, \boldsymbol{\psi}_j\right)_{X_h} \boldsymbol{\psi}_j \right\|_{X_h}^2, \tag{45}$$

such that

$$\left(\boldsymbol{\psi}_i, \boldsymbol{\psi}_j\right)_{X_h} = \delta_{ij}, \text{ for } 1 \le i \le d, 1 \le j \le i,$$

where

$$\|\boldsymbol{U}_i\|_{X_h} = \left[\|\nabla (u_x^{n_i})_h\|_0^2 + \left\|\nabla (u_y^{n_i})_h\right\|_0^2 + \|p_h^{n_i}\|_0^2\right]^{\frac{1}{2}}$$

in two dimensions or

$$\|\boldsymbol{U}_i\|_{X_h} = \left[\|\nabla (u_x^{n_i})_h\|_0^2 + \left\|\nabla (u_y^{n_i})_h\right\|_0^2 + \|\nabla (u_z^{n_i})_h\|_0^2 + \|p_h^{n_i}\|_0^2\right]^{\frac{1}{2}}$$

in three dimensions. A solution $\{\boldsymbol{\psi}_j\}_{j=1}^d = \{\boldsymbol{\psi}_{uj}, \psi_{pj}\}_{j=1}^d$ of (45) *is known as a POD basis of rank d.*

We also introduce the correlation matrix $\boldsymbol{K} = (K_{ij})_{L\times L} \in \mathbb{R}^{L\times L}$ here corresponding to the snapshots $\{\boldsymbol{U}_i\}_{i=1}^L$ by

$$K_{ij} = \frac{1}{L} \left(\boldsymbol{U}_i, \boldsymbol{U}_j\right)_{X_h}. \tag{46}$$

The matrix $\boldsymbol{K}$ is positive semi discrete and has rank $l \le L$. Then the solutions of (46) can be found in the following proposition.

Proposition 4.1 (Formula of POD basis[17])**.** *Let $\lambda_1 \ge \lambda_2 \ge \cdots \ge \lambda_l > 0$ denote the positive eigenvalues of $\boldsymbol{K}$ and $\boldsymbol{v}_1, \boldsymbol{v}_2, \ldots, \boldsymbol{v}_l$ the associated orthonormal eigenvectors. Then a POD basis of rank $d \le l$ is given by*

$$\boldsymbol{\psi}_i = \frac{1}{\sqrt{\lambda_i}} \sum_{j=1}^{L} (\boldsymbol{v}_i)_j \boldsymbol{U}_j, \tag{47}$$

where $(\boldsymbol{v}_i)_j$ *denotes the jth component of the eigenvector* $\boldsymbol{v}_i$*. Furthermore, the following error equation holds:*

$$\frac{1}{L}\sum_{i=1}^{L}\left\|\boldsymbol{U}_i-\sum_{j=1}^{d}\left(\boldsymbol{U}_i,\boldsymbol{\psi}_j\right)_{X_h}\boldsymbol{\psi}_j\right\|_{X_h}^2=\sum_{j=d+1}^{l}\lambda_j. \tag{48}$$

Let $X_d=\operatorname{span}\{\boldsymbol{\psi_1},\boldsymbol{\psi_2},\ldots,\boldsymbol{\psi_d}\}=U_d\times M_d$ with $U_d\subset U_h\subset U$ and $M_d\subset M_h\subset M$. Set the projection operator $P_h:U\to U_h$ (if P_h is restricted to projection from U_h to U_d, it is written as P_d) and L^2-projection $Q_h:M\to M_u$ (if Q_h is restricted to projection from M_h to M_d, it is written as Q_d), respectively. They satisfy

$$a\left(P_d\boldsymbol{u},\boldsymbol{v}_d\right)=a\left(\boldsymbol{u},\boldsymbol{v}_d\right)\quad\forall\boldsymbol{v}_d\in U_d, \tag{49}$$

and

$$\left(Q_dp,q_d\right)_0=\left(p,q_d\right)_0\quad\forall q_d\in M_d, \tag{50}$$

where $\boldsymbol{u}\in U_h$ and $p\in M_h$. Due to (49) and (50) the linear operators P_d and Q_d are well-defined and bounded:

$$\left\|\nabla(P_d\boldsymbol{u})\right\|_0\leq\left\|\nabla\boldsymbol{u}\right\|_0,\quad\forall\boldsymbol{u}\in U_h, \tag{51}$$

$$\left\|Q_dp\right\|_0\leq\left\|p\right\|_0,\quad\forall p\in M_h. \tag{52}$$

The P^d and Q^d defined above have the following properties:

Lemma 4.2 (Approximation properties of P_d and Q_d)**.** *For every* $d(1\leq d\leq l)$ *the projection operators* P_d *and* Q_d *satisfy*

$$\frac{1}{L}\sum_{i=1}^{L}\left\|\nabla\left(\boldsymbol{u}_h^{n_i}-P_d\boldsymbol{u}_h^{n_i}\right)\right\|_0^2\leq\sum_{j=d+1}^{l}\lambda_j, \tag{53}$$

$$\frac{1}{L}\sum_{i=1}^{L}\left\|\nabla\cdot\left(\boldsymbol{u}_h^{n_i}-P_d\boldsymbol{u}_h^{n_i}\right)\right\|_0^2\leq\sum_{j=d+1}^{l}\lambda_j, \tag{54}$$

$$\frac{1}{L}\sum_{i=1}^{L}\left\|\boldsymbol{u}_h^{n_i}-P_d\boldsymbol{u}_h^{n_i}\right\|_0^2\leq Ch^2\sum_{j=d+1}^{l}\lambda_j, \tag{55}$$

and

$$\frac{1}{L}\sum_{i=1}^{L}\left\|p_h^{n_i}-Q_dp_h^{n_i}\right\|_0^2\leq\sum_{j=d+1}^{l}\lambda_j. \tag{56}$$

Proof. We can get the conclusion according to the proof of [14] by Korn's inequality. □

Thus, we give the following semi discrete POD-ROM scheme through reduced space $X_d=U_d\times M_d$ for (8). Find $(\boldsymbol{u}_d^n,p_d^n)\in X_d$ such that

$$\begin{aligned}&\left(\boldsymbol{u}_d^n,p_d^n\right)=\left(R_d\boldsymbol{u}_h^n,Q_dp_h^n\right)\\&=\sum_{j=1}^{d}\left(\left(\nabla\boldsymbol{\psi}_{uj},\nabla\boldsymbol{u}_h^n\right)\boldsymbol{\psi}_{uj},\left(\psi_{pj},p_h^n\right)\psi_{pj}\right),0\leqslant n\leqslant L,\end{aligned} \tag{57}$$

$$(\rho\frac{\partial^2\boldsymbol{u}_d^n}{\partial t^2},\boldsymbol{v}_d)+a(\boldsymbol{u}_d^n,\boldsymbol{v}_d)+b(p_d^n,\boldsymbol{v}_d)=(\boldsymbol{f}^n,\boldsymbol{v}_d),\quad\forall\boldsymbol{v}_d\in U_d,\quad n\geq L+1, \tag{58}$$

$$b(\boldsymbol{u}_d^n,q_d)-c(p_d^n,q_d)=0,\quad\forall q_d\in M_d,\quad n\geq L+1, \tag{59}$$

where the POD-ROM solution $(\boldsymbol{u}_d^n, p_d^n) \in X_d$ is the projection of $(\boldsymbol{u}_h^n, p_h^n) \in X_h$ when $0 \leqslant n \leqslant L$. Here R_d is the classical Ritz projection operator defined in [14].

Remark 4.1. (57)-(59) *are formulas of POD-ROM. The number of total degrees of freedom of* (15) *is* N_h*, whereas the number of total degrees of freedom of* (58)-(59) *is* d*, and* $d \ll l \leqslant L \ll N_h$*.*

4.2. Error estimate of the semi discrete POD-ROM. We see that $X_d = U_d \times M_d \subset X_h = U_h \times M_h \subset X = U \times M$. Then it is obvious that the existence and uniqueness of (57)-(59). Now we derive the estimates of the semi discrete POD-ROM by the projection P_d and Q_d.

Theorem 4.3. *For* $t \geq 0$*, let* $(\boldsymbol{u}, p)$ *be the solution of the* (8) *and* $(\boldsymbol{u}_d, p_d)$ *be the solution of POD-ROM* (57)-(59)*. Assume that the solutions are smooth enough under the assumption of Theorem 3.3 and 3.4. Then there are constants* C_1*,* C_2*,* C_3 *and* C_4 *are independent on* h*, and* C_1, C_4 *are dependent on the* $\lambda^{-\frac{1}{2}}$ *such that*

$$\begin{aligned}&\left\|\rho^{\frac{1}{2}}(\boldsymbol{u}-\boldsymbol{u}_d)_t\right\|_{L^\infty(L^2)} + \left\|\lambda^{-\frac{1}{2}}(p-p_d)\right\|_{L^\infty(L^2)} + \left\|(2\mu)^{\frac{1}{2}}\nabla(\boldsymbol{u}-\boldsymbol{u}_d)\right\|_{L^\infty(L^2)}\\ &\leq C_1h^k + C_2h^k + C_3h^{k+1} + C_4\left(L\sum_{j=d+1}^{l}\lambda_j\right)^{1/2}.\end{aligned}$$

Proof. For simplicity, we denote $\boldsymbol{\theta} = \boldsymbol{u}_d - P_d\boldsymbol{u}_h, e = p_d - Q_dp_h, \boldsymbol{\sigma} = \boldsymbol{u}_h - P_d\boldsymbol{u}_h$, and $E = p_h - Q_dp_h$, where P_d and Q_d have been defined above. These definitions hold throughout the paper.

For $n \leq L$. Because $\boldsymbol{u}_d = R_d\boldsymbol{u}_h$ and $p_d = Q_d\boldsymbol{p}_h$. By the definition of strain operator ε, it can be seen as a linear combination of gradient operators. Hence we have $\boldsymbol{u}_d = P_d\boldsymbol{u}_h$ and $p_d = Q_d\boldsymbol{p}_h$ when $n = 1\cdots L$. Using the results (53)-(56) we can deduce that

$$\begin{aligned}&\left\|\rho^{\frac{1}{2}}(\boldsymbol{u}_h^n-\boldsymbol{u}_d^n)_t\right\|_{L^\infty(L^2)} + \left\|\lambda^{-\frac{1}{2}}(p_h^n-p_d^n)\right\|_{L^\infty(L^2)}\\ &+ \left\|(2\mu)^{\frac{1}{2}}\nabla(\boldsymbol{u}_h^n-\boldsymbol{u}_d^n)\right\|_{L^\infty(L^2)}\\ &\leq C\left(L\sum_{j=d+1}^{l}\lambda_j\right)^{1/2}, n = 1, 2, \ldots, L.\end{aligned} \tag{60}$$

For $n \geq L$. We use a similar argument of Theorem 3.5. First we subtract (58)-(59) from (15), and take $v_h = v_d, q_h = q_d$, we have

$$\begin{aligned}&(\rho\boldsymbol{\theta}_{tt}, \boldsymbol{v}_d) + a(\boldsymbol{\theta}, \boldsymbol{v}_d) + (e, \nabla\cdot\boldsymbol{v}_d)\\ &= (\rho\boldsymbol{\sigma}_{tt}, \boldsymbol{v}_d) + a(\boldsymbol{\sigma}, \boldsymbol{v}_d) + (E, \nabla\cdot\boldsymbol{v}_d) \quad \forall\boldsymbol{v}_d \in \boldsymbol{U}_d,\end{aligned} \tag{61}$$

$$\left(\lambda^{-1}e, q_d\right) - (\nabla\cdot\boldsymbol{\theta}, q_d) = \left(\lambda^{-1}E, q_d\right) - (\nabla\cdot\boldsymbol{\sigma}, q_d) \quad \forall q_d \in M_d, \tag{62}$$

then we set $\boldsymbol{v}_d = \boldsymbol{\theta}_t$, differentiate (62) about t, and take $q_d = e$. Adding two equations and combining with the definition of P_d and Q_d we infer

$$\begin{aligned}&\frac{1}{2}\Big(\frac{d}{dt}\left\|\rho^{\frac{1}{2}}\boldsymbol{\theta}_t\right\|^2_{L^2(\Omega)} + \frac{d}{dt}\left\|\lambda^{-\frac{1}{2}}e\right\|^2_{L^2(\Omega)} + \frac{d}{dt}\left\|(2\mu)^{\frac{1}{2}}\varepsilon(\boldsymbol{\theta})\right\|^2_{L^2(\Omega)}\Big)\\ &= (\rho\boldsymbol{\sigma}_{tt}, \boldsymbol{\theta}_t) + \left(\lambda^{-1}E_t, e\right) - (\nabla\cdot\boldsymbol{\sigma}_t, e).\end{aligned} \tag{63}$$

Then we use Cauchy-Schwarz's inequality and Young's inequality to bound the right side of (63)

$$\begin{aligned}
&\frac{d}{dt}\left\|\rho^{\frac{1}{2}}\boldsymbol{\theta}_t\right\|^2_{L^2(\Omega)}+\frac{d}{dt}\left\|\lambda^{-\frac{1}{2}}e\right\|^2_{L^2(\Omega)}+\frac{d}{dt}\left\|(2\mu)^{\frac{1}{2}}\varepsilon(\boldsymbol{\theta})\right\|^2_{L^2(\Omega)}\\
&\leq\left\|\rho^{\frac{1}{2}}\theta_t\right\|^2_{L^2(\Omega)}+\left\|\rho^{\frac{1}{2}}\boldsymbol{\sigma}_{tt}\right\|^2_{L^2(\Omega)}\\
&+C\left(\left\|\lambda^{-\frac{1}{2}}E_t\right\|^2_{L^2(\Omega)}+\left\|\lambda^{-\frac{1}{2}}\nabla\cdot\boldsymbol{\sigma}_t\right\|^2_{L^2(\Omega)}\right)+\left\|\lambda^{-\frac{1}{2}}e\right\|^2_{L^2(\Omega)},
\end{aligned}\tag{64}$$

integrating two sides of (64) form L to t and applying the Gronwall's inequality, by suitable initial values such that $\boldsymbol{\theta}_t(L)=\boldsymbol{\theta}(L)=e(L)=0$, we infer

$$\begin{aligned}
&\left\|\rho^{\frac{1}{2}}\boldsymbol{\theta}_t\right\|^2_{L^2(\Omega)}(t)+\left\|\lambda^{-\frac{1}{2}}e\right\|^2_{L^2(\Omega)}(t)+\left\|(2\mu)^{\frac{1}{2}}\varepsilon(\boldsymbol{\theta})\right\|^2_{L^2(\Omega)}(t)\\
&\leq C\int_L^t\left(\left\|\rho^{\frac{1}{2}}\boldsymbol{\sigma}_{tt}\right\|^2_{L^2(\Omega)}+\left\|\lambda^{-\frac{1}{2}}E_t\right\|^2_{L^2(\Omega)}+\left\|\lambda^{-\frac{1}{2}}\nabla\cdot\boldsymbol{\sigma}_t\right\|^2_{L^2(\Omega)}\right),
\end{aligned}\tag{65}$$

then we bound the first term on the right side by using the properties of projection operators (53)-(56):

$$\begin{cases}
\left\|\rho^{\frac{1}{2}}\boldsymbol{\sigma}_{tt}\right\|^2_{L^2(\Omega)}\leq C_1h^2\left(L\sum_{j=d+1}^{l}\lambda_j\right)\\
\left\|\lambda^{-\frac{1}{2}}E_t\right\|^2_{L^2(\Omega)}\leq C_2\left(L\sum_{j=d+1}^{l}\lambda_j\right)\\
\left\|\lambda^{-\frac{1}{2}}\nabla\cdot\boldsymbol{\sigma}_t\right\|^2_{L^2(\Omega)}\leq C_3\left(L\sum_{j=d+1}^{l}\lambda_j\right)
\end{cases},\tag{66}$$

where C_1, C_2 and C_3 are independent on h, and C_2, C_3 are dependent on λ^{-1}.

Taking the maximum over all time levels of (65), using the approximation properties of $\boldsymbol{\sigma}_t$, E and $\varepsilon(\boldsymbol{\sigma})$, we infer

$$\begin{aligned}
&\left\|\rho^{\frac{1}{2}}(\boldsymbol{u}_h-\boldsymbol{u}_d)_t\right\|^2_{L^\infty(L^2)}+\left\|\lambda^{-\frac{1}{2}}(p_h-p_d)\right\|^2_{L^\infty(L^2)}\\
&+\left\|(2\mu)^{\frac{1}{2}}\varepsilon(\boldsymbol{u}_h-\boldsymbol{u}_d)\right\|^2_{L^\infty(L^2)}\leq C\left(L\sum_{j=d+1}^{l}\lambda_j\right),
\end{aligned}\tag{67}$$

where C is dependent on λ^{-1}. Finally, we obtain the error estimate between $(\boldsymbol{u},p)$ and $(\boldsymbol{u}_d,p_d)$ by using the Theorem 3.3 and triangle inequality. □

Next, we give the L^2 error estimate between $\boldsymbol{u}$ and $\boldsymbol{u}_d$ by the similar argument of Theorem 3.5.

Theorem 4.4. *For $t\geq 0$, let $(\boldsymbol{u},p)$ be the solution of (8) and $(\boldsymbol{u}_d,p_d)$ be the solution of (58)-(59). Assume that solutions are smooth enough. Under the same assumption of Theorem 3.5. Then there are constants C_1, C_2 and C_3 independent of h, and C_1, C_3 are dependent on $\lambda^{-\frac{1}{2}}$ such that*

$$\left\|\rho^{\frac{1}{2}}(\boldsymbol{u}-\boldsymbol{u}_d)\right\|_{L^\infty(L^2)}\leq C_1h^k+C_2h^{k+1}+C_3\left(L\sum_{j=d+1}^{l}\lambda_j\right)^{1/2}.$$

Proof. For $n \leq L$, we have

$$\left\|\rho^{\frac{1}{2}}(\boldsymbol{u}_h^n - \boldsymbol{u}_d^n)\right\|_{L^\infty(L^2)} \leq Ch\left(L\sum_{j=d+1}^{l}\lambda_j\right)^{1/2}, n = 1, 2, \ldots, L, \tag{68}$$

according to (55). For $n \geq L$, we begin with the following error equation

$$(\rho\boldsymbol{\theta}_{tt}, \boldsymbol{v}_d) + a(\boldsymbol{\theta}, \boldsymbol{v}_d) + (e, \nabla\cdot\boldsymbol{v}_d) = (\rho\boldsymbol{\sigma}_{tt}, \boldsymbol{v}_d) \quad \forall \boldsymbol{v}_d \in \boldsymbol{U}_d, \tag{69}$$

$$\left(\lambda^{-1}e, q_d\right) - (\nabla\cdot\boldsymbol{\theta}, q_d) = \left(\lambda^{-1}E, q_d\right) - (\nabla\cdot\boldsymbol{\sigma}, q_d) \quad \forall q_d \in M_d, \tag{70}$$

If we integrate (69) from L to t, with initial conditions $\boldsymbol{\theta}_t(L) = 0$. Then we set $\boldsymbol{v}_d = \boldsymbol{\theta}, \phi = \int_L^t e(s)ds$ and take $q_d = \phi$ in (70). We have

$$(\rho\boldsymbol{\theta}_t, \boldsymbol{\theta}) + \left(\int_L^t \varepsilon(\boldsymbol{\theta}), \varepsilon(\boldsymbol{\theta})\right) + (\phi, \nabla\cdot\boldsymbol{\theta}) = (\rho\boldsymbol{\sigma}_t, \boldsymbol{\theta}) - (\rho\boldsymbol{\sigma}_t(L), \boldsymbol{\theta}), \tag{71}$$

$$\left(\lambda^{-1}e, \phi\right) - (\nabla\cdot\boldsymbol{\theta}, \phi) = \left(\lambda^{-1}E, \phi\right) - (\nabla\cdot\boldsymbol{\sigma}, \phi), \tag{72}$$

adding (71) and (72) gives

$$\begin{aligned}&(\rho\boldsymbol{\theta}_t, \boldsymbol{\theta}) + \left(\int_L^t \varepsilon(\boldsymbol{\theta}), \varepsilon(\boldsymbol{\theta})\right) + \left(\lambda^{-1}e, \phi\right)\\ &= (\rho\boldsymbol{\sigma}_t, \boldsymbol{\theta}) - (\rho\boldsymbol{\sigma}_t(L), \boldsymbol{\theta}) + \left(\lambda^{-1}E, \phi\right) - (\nabla\cdot\boldsymbol{\sigma}, \phi).\end{aligned} \tag{73}$$

Then we set $\mathcal{N} = \int_L^t \varepsilon(\theta(s))ds$ and suitable initial conditions $\varepsilon(\theta(L)) = 0$ and $e(L) = 0$.

$$\begin{aligned}&(\rho\boldsymbol{\theta}_t, \boldsymbol{\theta}) + (\mathcal{N}, \mathcal{N}_t) + \left(\lambda^{-1}\phi_t, \phi\right)\\ &= (\rho\boldsymbol{\sigma}_t, \boldsymbol{\theta}) - (\rho\boldsymbol{\sigma}_t(L), \boldsymbol{\theta}) + \left(\lambda^{-1}E, \phi\right) - (\nabla\cdot\boldsymbol{\sigma}, \phi),\end{aligned} \tag{74}$$

using Cauchy-Schwarz's inequality and Young's inequality gives

$$\begin{aligned}&\frac{d}{dt}\left\|\rho^{\frac{1}{2}}\boldsymbol{\theta}\right\|_{L^2(\Omega)}^2 + \frac{d}{dt}\left\|\lambda^{-\frac{1}{2}}\phi\right\|_{L^2(\Omega)}^2 + \frac{d}{dt}\left\|(2\mu)^{\frac{1}{2}}\mathcal{N}\right\|_{L^2(\Omega)}^2\\ &\leq \left\|\rho^{\frac{1}{2}}\boldsymbol{\theta}\right\|_{L^2(\Omega)}^2 + C(\left\|\rho^{\frac{1}{2}}\boldsymbol{\sigma}_t\right\|_{L^2(\Omega)}^2 + \left\|\rho^{\frac{1}{2}}\boldsymbol{\sigma}_t(L)\right\|_{L^2(\Omega)}^2)\\ &+ C\left(\left\|\lambda^{-\frac{1}{2}}E\right\|_{L^2(\Omega)}^2 + \left\|\lambda^{-\frac{1}{2}}\nabla\cdot\boldsymbol{\sigma}\right\|_{L^2(\Omega)}^2\right) + \left\|\lambda^{-\frac{1}{2}}\phi\right\|_{L^2(\Omega)}^2.\end{aligned} \tag{75}$$

We integrate both sides of the equation (75) from L to t and apply Gronwall's inequality, noting that $\phi(L) = 0$ and $\boldsymbol{\theta}(L) = 0$. Then we obtain

$$\begin{aligned}&\left\|\rho^{\frac{1}{2}}\boldsymbol{\theta}\right\|_{L^2(\Omega)}^2(t) + \left\|\lambda^{-\frac{1}{2}}\phi\right\|_{L^2(\Omega)}^2(t) + \left\|(2\mu)^{\frac{1}{2}}\mathcal{N}\right\|_{L^2(\Omega)}^2(t)\\ &\leq C\int_L^t(\left\|\rho^{\frac{1}{2}}\boldsymbol{\sigma}_s\right\|_{L^2(\Omega)}^2 + \left\|\rho^{\frac{1}{2}}\boldsymbol{\sigma}_s(L)\right\|_{L^2(\Omega)}^2\\ &+ \left\|\lambda^{-\frac{1}{2}}E\right\|_{L^2(\Omega)}^2 + \left\|\lambda^{-\frac{1}{2}}\nabla\cdot\boldsymbol{\sigma}\right\|_{L^2(\Omega)}^2)ds,\end{aligned} \tag{76}$$

then we take the maximum over all t, by the similar argument in Theorem 3.4 we infer

$$\begin{aligned}
&\left\|\rho^{\frac{1}{2}}\boldsymbol{\theta}\right\|^2_{L^2(\Omega)}(t)+\left\|\lambda^{-\frac{1}{2}}\phi\right\|^2_{L^2(\Omega)}(t)+\left\|(2\mu)^{\frac{1}{2}}\mathcal{N}\right\|^2_{L^2(\Omega)}(t)\\
&\leq C\left\|\rho^{\frac{1}{2}}\boldsymbol{\sigma}_t\right\|^2_{L^2(L^2)}+Ct\left\|\rho^{\frac{1}{2}}\boldsymbol{\sigma}_t(L)\right\|^2_{L^2(\Omega)}\\
&+C\left\|\lambda^{-\frac{1}{2}}E\right\|^2_{L^2(L^2)}+C\left\|\lambda^{-\frac{1}{2}}\nabla\cdot\boldsymbol{\sigma}\right\|^2_{L^2(L^2)}. \qquad (77)
\end{aligned}$$

We estimate the right side of (77) by using properties of projection P_d and Q_d (53)-(56). The final result is obtained by Theorem 3.5 and triangle inequality. □

4.3. Error estimate of the fully discrete POD-ROM. In this section, we give the fully discrete POD-ROM as follows: Find $\boldsymbol{u}_d^{n+1}$ and p_d^{n+1} such that

$$\begin{cases}
\left(\rho\partial_t^2\boldsymbol{u}_d^n,\boldsymbol{v}_d\right)+a\left(\boldsymbol{u}_h^{n,\frac{1}{2}},\boldsymbol{v}_d\right)+b\left(p_d^{n,\frac{1}{2}},\boldsymbol{v}_d\right)\\
=\left(\boldsymbol{f}^{n,\frac{1}{2}},\boldsymbol{v}_d\right),\forall\boldsymbol{v}_d\in U_d,n>L,\\
b\left(\boldsymbol{u}_d^{n+\frac{1}{2}},q_d\right)-c\left(p_d^{n+\frac{1}{2}},q_d\right)=0,\forall q_d\in M_d,n>L,\\
\left(\boldsymbol{u}_d^n,\boldsymbol{v}_d\right)=\left(P_du_h^n,\boldsymbol{v}_d\right),n\leq L,\\
\left(p_d^n,q_d\right)=\left(Q_dp_h^n,q_d\right),n\leq L,
\end{cases} \qquad (78)$$

The scheme is unconditionally stable, and the error estimate is as follows:

Theorem 4.5. *Assume $(\boldsymbol{u},p)$ are the solution of (8), $(\boldsymbol{u}_d^n,p_d^n)$ are the solution of (78), under the assumption of Theorem 3.7, we have the following result:*

$$\begin{aligned}
&\|\rho^{\frac{1}{2}}(\boldsymbol{u}(t_n)-\boldsymbol{u}_d^n)\|_{l^\infty(L^2)}+\|\lambda^{-\frac{1}{2}}(p(t_n)-p_d^n)\|_{l^\infty(L^2)}+\|\nabla(\boldsymbol{u}(t_n)-\boldsymbol{u}_d^n)\|_{l^\infty(L^2)}\\
&\leq C(h^k+\Delta t^2+(L\sum_{j=d+1}^{l}\lambda_j)^{1/2}),
\end{aligned}$$

where C is independent on h and Δt, and is dependent on $\lambda^{-\frac{1}{2}}$.

Proof. For $n\leq L$, we directly have

$$\begin{aligned}
&\|\rho^{\frac{1}{2}}(\boldsymbol{u}_h^n-\boldsymbol{u}_d^n)\|_{l^\infty(L^2)}+\|\lambda^{-\frac{1}{2}}(p_h^n-p_d^n)\|_{l^\infty(L^2)}\\
&+\|\nabla(\boldsymbol{u}_h^n-\boldsymbol{u}_d^n)\|_{l^\infty(L^2)}\leq C\left(L\sum_{j=d+1}^{l}\lambda_j\right)^{1/2}.
\end{aligned}$$

For $n\geq L$, subtracting (29)-(30) from (78), we infer

$$\left(\rho\partial_t^2\boldsymbol{\theta}^n,\boldsymbol{v}_d\right)+a(\boldsymbol{\theta}^{n,\frac{1}{2}},\boldsymbol{v}_d)+b(e^{n,\frac{1}{2}},\boldsymbol{v}_d)=\left(\rho\partial_t^2\boldsymbol{\sigma},\boldsymbol{v}_d\right)\quad\forall\boldsymbol{v}_d\in\boldsymbol{U}_d, \qquad (79)$$

$$\left(\lambda^{-1}e^{n+\frac{1}{2}},q_d\right)-b(q_d,\boldsymbol{\theta}^{n+\frac{1}{2}})=\left(\lambda^{-1}E^{n+\frac{1}{2}},q_d\right)-b(q_d,\boldsymbol{\sigma}^{n+\frac{1}{2}})\quad\forall q_d\in M_d, \qquad (80)$$

using the technique the proof of the Theorem 3.7, we introduce the following variables:

$$\phi_d^n=\Delta t\sum_{i=L}^{n-1}e^{i+\frac{1}{2}},\quad\phi_d^L=0,\quad\psi_d^n=\Delta t\sum_{i=L}^{n-1}\boldsymbol{\theta}^{i+\frac{1}{2}},\quad\psi_d^L=0,$$

noting that

$$\phi_d^{n+\frac{1}{2}}=\frac{\Delta t}{2}e^{L+\frac{1}{2}}+\frac{\Delta t}{2}\sum_{i=L+1}^{n}(e^{i+\frac{1}{2}}+e^{i-\frac{1}{2}}),$$

$$\psi_d^{n+\frac{1}{2}} = \frac{\Delta t}{2}\boldsymbol{\theta}^{L+\frac{1}{2}} + \frac{\Delta t}{2}\sum_{i=L+1}^{n}(\boldsymbol{\theta}^{i+\frac{1}{2}} + \boldsymbol{\theta}^{i-\frac{1}{2}}).$$

Rewriting (79) as

$$\begin{aligned}
&(\rho\partial_t^2\boldsymbol{\theta}^n, \boldsymbol{v}_d) + \frac{1}{2}a(\boldsymbol{\theta}^{n+\frac{1}{2}} + \boldsymbol{\theta}^{n-\frac{1}{2}}, \boldsymbol{v}_d) + \frac{\Delta t^2}{4}a(\partial_t^2\boldsymbol{\theta}^n, \boldsymbol{v}_d)\\
&+ \frac{1}{2}b(e^{n+\frac{1}{2}} + e^{n-\frac{1}{2}}, \boldsymbol{v}_d) + \frac{\Delta t^2}{4}b(\partial_t^2 e^n, \boldsymbol{v}_d)\\
&= (\rho\partial_t^2\boldsymbol{\sigma}^2, \boldsymbol{v}_d). \qquad (81)
\end{aligned}$$

Summing over time levels from $L+1$ to n we infer that:

$$\begin{aligned}
&(\rho\partial_t\boldsymbol{\theta}^{n+\frac{1}{2}} - \rho\partial_t\boldsymbol{\theta}^{L+\frac{1}{2}}, \boldsymbol{v}_d) + \frac{\Delta t}{2}\sum_{i=L+1}^{n}a(\boldsymbol{\theta}^{i+\frac{1}{2}} + \boldsymbol{\theta}^{i-\frac{1}{2}}, \boldsymbol{v}_d)\\
&+ \frac{\Delta t^2}{4}a(\partial_t\boldsymbol{\theta}^{n+\frac{1}{2}} - \partial_t\boldsymbol{\theta}^{L+\frac{1}{2}}, \boldsymbol{v}_d)\\
&+ \frac{\Delta t}{2}\sum_{i=L+1}^{n}b(e^{i+\frac{1}{2}} + e^{i-\frac{1}{2}}, \boldsymbol{v}_d) + \frac{\Delta t^2}{4}b(\partial_t e^{n+\frac{1}{2}} - \partial_t e^{L+\frac{1}{2}}, \boldsymbol{v}_d)\\
&= (\rho\partial_t\boldsymbol{\sigma}^{n+\frac{1}{2}} - \rho\partial_t\boldsymbol{\sigma}^{L+\frac{1}{2}}, \boldsymbol{v}_d). \qquad (82)
\end{aligned}$$

In addition, we take $n = L$ in (79). Combing with the initial condition we infer that

$$(\rho\frac{\boldsymbol{\theta}^{L+1}}{\Delta t^2}, \boldsymbol{v}_d) + a(\frac{\boldsymbol{\theta}^{L+1}}{2}, \boldsymbol{v}_d) + b(\frac{e^{L+1}}{2}, \boldsymbol{v}_d) = (\rho\frac{\boldsymbol{\sigma}^{L+1}}{\Delta t^2}, \boldsymbol{v}_d). \qquad (83)$$

Multiplying both sides by Δt, noting $\frac{\boldsymbol{\theta}^{L+1}}{\Delta t} = \partial_t\boldsymbol{\theta}^{L+\frac{1}{2}}$, $\frac{\boldsymbol{\sigma}^{L+1}}{\Delta t} = \partial_t\boldsymbol{\sigma}^{L+\frac{1}{2}}$, $\frac{\Delta t}{2}\boldsymbol{\theta}^{L+1} = \frac{\Delta t^2}{2}\partial_t\boldsymbol{\theta}^{L+1}$, $\frac{\Delta t}{2}e^{L+1} = \frac{\Delta t^2}{2}\partial_t e^{L+1}$, we obtain

$$\begin{aligned}
&(-\rho\partial_t\boldsymbol{\theta}^{L+\frac{1}{2}}, \boldsymbol{v}_d)\\
&= a(\frac{\Delta t^2}{2}\partial_t\boldsymbol{\theta}^{L+1}, \boldsymbol{v}_d) + b(\frac{\Delta t^2}{2}\partial_t e^{L+1}, \boldsymbol{v}_d) - (\rho\partial_t\boldsymbol{\sigma}^{L+\frac{1}{2}}, \boldsymbol{v}_d). \qquad (84)
\end{aligned}$$

Taking (84) into (82), noting that $\frac{\Delta t^2}{4}\partial_t\boldsymbol{\theta}^{L+\frac{1}{2}} = \frac{\Delta t}{2}\boldsymbol{\theta}^{L+\frac{1}{2}}$, $\frac{\Delta t^2}{4}\partial_t e^{L+\frac{1}{2}} = \frac{\Delta t}{2}e^{L+\frac{1}{2}}$ and the definitions of $\phi_d^{n+\frac{1}{2}}, \psi_d^{n+\frac{1}{2}}$, we have the result

$$\begin{aligned}
&(\rho\partial_t\boldsymbol{\theta}^{n+\frac{1}{2}}, \boldsymbol{v}_d) + \frac{\Delta t^2}{4}a(\partial_t\boldsymbol{\theta}^{n+\frac{1}{2}}, \boldsymbol{v}_d) + a(\psi_d^{n+\frac{1}{2}}, \boldsymbol{v}_d)\\
&+ \frac{\Delta t^2}{4}b(\partial_t e^{n+\frac{1}{2}}, \boldsymbol{v}_d) + b(\phi_d^{n+\frac{1}{2}}, \boldsymbol{v}_d) = (\rho\partial_t\boldsymbol{\sigma}^{n+\frac{1}{2}}, \boldsymbol{v}_d), \qquad (85)
\end{aligned}$$

The following proof process is similar to (41)-(43), so we obtain

$$\begin{aligned}
&\|\rho^{\frac{1}{2}}\boldsymbol{\theta}\|_{l^\infty(L^2)}^2 + \|\lambda^{-\frac{1}{2}}\phi_d\|_{l^\infty(L^2)}^2 + \|\lambda^{-\frac{1}{2}}\psi_d\|_{l^\infty(H^1)}^2\\
&\leq C\left(\|\lambda^{-\frac{1}{2}}E\|_{l^\infty(L^2)}^2 + \Delta t^2(\sum_{i=0}^{N-1}\|\rho\partial_t\boldsymbol{\sigma}^{i+\frac{1}{2}}\|_{L^2}^2)\right). \qquad (86)
\end{aligned}$$

Using the approximation property of E and $\boldsymbol{\sigma}$ and the same technique as proved (43), we get the following result:

$$\|\rho^{\frac{1}{2}}(\boldsymbol{u}_h(t^n)-\boldsymbol{u}_d^n)\|_{l^\infty(L^2)}+\|\lambda^{-\frac{1}{2}}(p_h(t^n)-p_d^n)\|_{l^\infty(L^2)}$$
$$+\|\nabla(\boldsymbol{u}_h(t^n)-\boldsymbol{u}_d^n)\|_{l^\infty(L^2)}\leq C(\Delta t^2+(L\sum_{j=d+1}^{l}\lambda_j)^{1/2}).$$

Then using the result of (43) and triangle inequality, combining with similar proof of Theorem 3.7, we complete the proof. □

4.4. Algorithm. The algorithm of the POD-ROM for the elastic wave equation is as follows:

Algorithm 1 POD-ROM algorithm

Step 1. Using the MFE method to obtain the L solution $(\boldsymbol{u}_h, p_h)$ of snapshot.
Computing (29)-(33) yields solutions $\boldsymbol{u}_h^n(n=1,2,\cdots,L)$.
Step 2. Assemble the snapshot matrix A
The snapshot matrix $\boldsymbol{A}=(A_{ij})_{L\times L}$, where $A_{ij}=\left[\left(\nabla\boldsymbol{u}_h^i,\nabla\boldsymbol{u}_h^j\right)+\left(p_h^i,p_h^j\right)\right]/L$.
Step 3. Calculating eigenvalues and eigenvectors of A
Obtaining the eigenvalues $\lambda_1\geqslant\lambda_2\geqslant\cdots\geqslant\lambda_l>0\,(l=\dim\{u_h^n:1\leqslant n\leqslant L\})$ of $\boldsymbol{A}$ and the corresponding eigenvectors $\boldsymbol{v}^j=\left(a_1^j,a_2^j,\cdots,a_L^j\right)^T(j=1,2,\cdots,l)$.
Step 4. Obtain the number of POD basis
We set the error $\delta=O\left(\Delta t^2,h^k\right)$ needed, then we decide the optimal number d of POD bases by $\left(L\sum_{j=d+1}^{l}\lambda_j\right)^{1/2}\leqslant\delta$.
Step 5. Calculating the POD basis
The POD basis calculated by $\left(\boldsymbol{\psi}_{uj}(x,y),\psi_{pj}(x,y)\right)=\sum_{i=1}^{L}a_i^j\left(\boldsymbol{u}_h^i,p_h^i\right)/\sqrt{L\lambda_j}(j=1,2,\cdots,d)$.
Step 6. Using the POD-ROM to obtain the reduced solution $\boldsymbol{u}_d$
Using (78) to compute.
Step 7. Decide whether to update the POD basis
If $\left\|u_d^{n-1}-u_d^n\right\|_0\geqslant\left\|u_d^n-u_d^{n+1}\right\|_0$ and $\left\|p_d^{n-1}-p_d^n\right\|_0\geqslant\left\|p_d^n-p_d^{n+1}\right\|_0(n=L,L+1,\cdots,N-1)$;
Then $(\boldsymbol{u}_d^n,p_d^n)\,(n=1,2,\cdots,N)$ are the solutions to the POD-ROM method that satisfy the accuracy requirement.
Else if $\left\|u_d^{n-1}-u_d^n\right\|_0<\left\|u_d^n-u_d^{n+1}\right\|_0$ or $\left\|p_d^{n-1}-p_d^n\right\|_0<\left\|p_d^n-p_d^{n+1}\right\|_0(n=L,L+1,\cdots,N-1)$
let $\left(\boldsymbol{u}_h^i,p_h^i\right)=\left(\boldsymbol{u}_d^i,p_d^i\right)(i=n-L,n-L-1,\cdots,n-1)$, return to **Step 2**.

5. Numerical experiments

In this section, we test the FOM and the POD-ROM of the elastic wave equation to validate the theoretical analysis. That is, testing based on FOM (29)-(33) and POD-ROM (78). In addition, we solve the discrete systems of equations with a direct solver. $\mathcal{T}_h$ is taken as uniform triangulation in 2D or uniform tetrahedron in 3D. We use the approximation space as the Mini's element space for calculation.

5.1. Locking-free. In this part, we test POD-ROM's locking-free ability. For the 2D example, the computational domain is $\Omega=(0,1)^2$ with a partition of triangles.

TABLE 1. 2D example, $\lambda = 1$.

(A) The FOM

h	$\|\boldsymbol{u} - \boldsymbol{u}_h\|_0$	Rate	$\|\boldsymbol{u} - \boldsymbol{u}_h\|_1$	Rate
1/2	1.5530e-02	0	1.2443e-01	0
1/4	3.6977e-03	2.07	6.3403e-02	0.97
1/8	9.0460e-04	2.03	3.1800e-02	1.00
1/16	2.2369e-04	2.02	1.5898e-02	1.00
1/32	5.5495e-05	2.01	7.9453e-03	1.00
1/64	1.3584e-05	2.03	3.9714e-03	1.00

(B) The POD-ROM

h	$\|\boldsymbol{u} - \boldsymbol{u}_d\|_0$	Rate	$\|\boldsymbol{u} - \boldsymbol{u}_d\|_1$	Rate
1/2	1.5445e-02	0	1.2433e-01	0
1/4	3.8091e-03	2.02	6.3245e-02	0.98
1/8	9.4096e-04	2.02	3.1786e-02	0.99
1/16	2.3656e-04	1.99	1.5895e-02	1.00
1/32	5.9322e-05	2.00	7.9451e-03	1.00
1/64	1.4790e-05	2.00	3.9714e-03	1.00

The exact solution of displacement is given by

$$\boldsymbol{u} = \begin{bmatrix} \sin x \sin y + \frac{1}{\lambda} x \\ \cos x \cos y + \frac{1}{\lambda} y \end{bmatrix} \sin t.$$

For the 3D example, the computational domain is $\Omega = (0,1)^3$ with a partition of tetrahedrons. The exact solution of displacement is given by

$$\boldsymbol{u} = \begin{bmatrix} 2 \sin x \sin y \sin z + \frac{1}{\lambda} x \\ \cos x \cos y \sin z + \frac{1}{\lambda} y \\ \cos z + \frac{1}{\lambda} z \end{bmatrix} \sin t.$$

We notice $\nabla \cdot u \to 0$ as $\lambda \to \infty$. The corresponding source term can be given by (1). We find the two solutions are sensitive to volumetric locking for a large λ. The following parameters are set for the test: $\rho = 1$, $\mu = 1$, the total time is $10s$, the time step is $0.01s$, and the mesh size is $h = 1/2, 1/4, 1/8, 1/16, 1/32, 1/64$ in the 2D test and $h = 1/2, 1/4, 1/8, 1/16$ in the 3D test. The number of snapshots is $L = 20$, $L = 30$ and $L = 50$ under $\lambda = 1, 10^3, 10^6$ in the 2D test. The number of snapshots is $L = 50$, $L = 70$ and $L = 100$ under $\lambda = 1, 10^3, 10^6$ in the 3D test.

The convergence rate of the two-dimensional test of the POD-ROM under different λ is demonstrated in Table 1-Table 3. The convergence rate of the three-dimensional test of the POD-ROM under different λ is demonstrated in Table 4-Table 6. The results showed that the POD-ROM is able to reach the convergence order of theoretical analysis and is locking-free when $\lambda \to \infty$.

5.2. Computational efficiency. In this part, we compare the computational efficiency of POD-ROM and FOM. The two-dimensional area is $\Omega = [0, 1/4] \times [0, 1/4]$ and the three-dimensional area is $\Omega = [0, 1/4] \times [0, 1/4] \times [0, 1/4]$. The two-dimensional exact solution is

$$\boldsymbol{u} = \begin{bmatrix} -4x(x-1)y(y-1) \\ 4x(x-1)y(y-1) \end{bmatrix} \sin(t),$$

TABLE 2. 2D example, $\lambda = 10^3$.

(A) The FOM

h	$\|\boldsymbol{u} - \boldsymbol{u}_h\|_0$	Rate	$\|\boldsymbol{u} - \boldsymbol{u}_h\|_1$	Rate
1/2	1.4250e-02	0	1.2978e-01	0
1/4	3.2820e-03	2.12	6.5085e-02	1.00
1/8	7.5909e-04	2.11	3.2178e-02	1.02
1/16	1.8667e-04	2.02	1.5984e-02	1.01
1/32	4.6394e-05	2.01	7.9653e-03	1.00
1/64	1.1537e-05	2.01	3.9761e-03	1.00

(B) The POD-ROM

h	$\|\boldsymbol{u} - \boldsymbol{u}_d\|_0$	Rate	$\|\boldsymbol{u} - \boldsymbol{u}_d\|_1$	Rate
1/2	3.3769e-01	0	3.8813e-01	0
1/4	3.5758e-02	3.24	8.1616e-02	2.25
1/8	1.0928e-03	5.03	3.2161e-02	1.34
1/16	2.0345e-04	2.43	1.5985e-02	1.01
1/32	4.9845e-05	2.03	7.9658e-03	1.00
1/64	1.1778e-05	2.08	3.9763e-03	1.00

TABLE 3. 2D example, $\lambda = 10^6$.

(A) The FOM

h	$\|\boldsymbol{u} - \boldsymbol{u}_h\|_0$	Rate	$\|\boldsymbol{u} - \boldsymbol{u}_h\|_1$	Rate
1/2	1.4360e-02	0	1.2950e-01	0
1/4	3.2800e-03	2.13	6.4995e-02	0.99
1/8	7.6541e-04	2.10	3.2169e-02	1.01
1/16	1.8675e-04	2.03	1.5985e-02	1.01
1/32	4.6537e-05	2.00	7.9654e-03	1.00
1/64	1.1548e-05	2.01	3.9761e-03	1.00

(B) The POD-ROM

h	$\|\boldsymbol{u} - \boldsymbol{u}_d\|_0$	Rate	$\|\boldsymbol{u} - \boldsymbol{u}_d\|_1$	Rate
1/2	1.3962e-02	0	1.3171e-01	0
1/4	3.1809e-03	2.13	6.5027e-02	1.02
1/8	7.3533e-04	2.11	3.2179e-02	1.01
1/16	1.7913e-04	2.04	1.5986e-02	1.01
1/32	4.7497e-05	1.92	7.9659e-03	1.00
1/64	1.1144e-05	2.09	3.9763e-03	1.00

the three-dimensional exact solution is

$$\boldsymbol{u} = \begin{bmatrix} \cos(\pi z)\sin(\pi x)\sin(\pi y)\sin(\pi z) \\ \cos(\pi x)\sin(\pi x)\sin(\pi y)\sin(\pi z) \\ \cos(\pi y)\sin(\pi x)\sin(\pi y)\sin(\pi z) \end{bmatrix} \sin(t),$$

TABLE 4. 3D example, $\lambda = 1$.

(A) The FOM

h	$\|\boldsymbol{u} - \boldsymbol{u}_h\|_0$	Rate	$\|\boldsymbol{u} - \boldsymbol{u}_h\|_1$	Rate
1/2	3.3775e-02	0	2.7267e-01	0
1/4	8.3384e-03	2.02	1.3762e-01	0.99
1/8	2.0316e-03	2.04	6.8966e-02	1.00
1/16	5.0774e-04	2.00	3.4485e-02	1.00

(B) The POD-ROM

h	$\|\boldsymbol{u} - \boldsymbol{u}_d\|_0$	Rate	$\|\boldsymbol{u} - \boldsymbol{u}_d\|_1$	Rate
1/2	3.3779e-02	0	2.7266e-01	0
1/4	8.3816e-03	2.01	1.3761e-01	0.99
1/8	2.0568e-03	2.03	6.8958e-02	1.00
1/16	5.0779e-04	2.02	3.4485e-02	1.00

TABLE 5. 3D example, $\lambda = 10^3$.

(A) The FOM

h	$\|\boldsymbol{u} - \boldsymbol{u}_h\|_0$	Rate	$\|\boldsymbol{u} - \boldsymbol{u}_h\|_1$	Rate
1/2	3.2819e-02	0	2.7365e-01	0
1/4	9.5460e-03	1.78	1.5943e-01	0.78
1/8	2.2776e-03	2.08	7.8412e-02	1.02
1/16	5.2022e-04	2.13	3.7627e-02	1.06

(B) The POD-ROM

h	$\|\boldsymbol{u} - \boldsymbol{u}_d\|_0$	Rate	$\|\boldsymbol{u} - \boldsymbol{u}_d\|_1$	Rate
1/2	3.0350e-02	0	2.7841e-01	0
1/4	9.5007e-03	1.68	1.5905e-01	0.81
1/8	2.3166e-03	2.04	7.9009e-02	1.00
1/16	5.2051e-04	2.15	3.7679e-02	1.07

We set $\rho = 1$, $\lambda = 1$, $\mu = 1$. The number of snapshots $L = 20$ in the two-dimensional case and $L = 50$ in the three-dimensional case. The record time $T = 1s$ and the time step $\Delta t = 0.001s$. Tables 7-8 show the comparison of computing efficiency between POD-ROM and FOM under different grid sizes. In addition, we set $T = 1 - 5s$. In two dimensions, the grid scale is $h = 1/32$, and in three dimensions, the grid-scale is $h = 1/8$. Tables 9-10 show the CPU time required for ROM and FOM at different recording times.

It can be seen that ROM can effectively improve computing efficiency while maintaining accuracy. If the grid is finer and the time calculation time is longer, the effect will be more obvious.

5.3. Point source problem. In this section, we investigate a point source problem inspired by [29] where the analytical solution is not easily obtainable. The

TABLE 6. 3D example, $\lambda = 10^6$.

(A) The FOM

h	$\|\boldsymbol{u} - \boldsymbol{u}_h\|_0$	Rate	$\|\boldsymbol{u} - \boldsymbol{u}_h\|_1$	Rate
1/2	3.1154e-02	0	3.0422e-01	0
1/4	1.0143e-02	1.62	1.7427e-01	0.80
1/8	2.4997e-03	2.02	8.4743e-02	1.04
1/16	6.2287e-04	2.00	4.1377e-02	1.03

(B) The POD-ROM

h	$\|\boldsymbol{u} - \boldsymbol{u}_d\|_0$	Rate	$\|\boldsymbol{u} - \boldsymbol{u}_d\|_1$	Rate
1/2	3.4110e-02	0	3.0111e-01	0
1/4	1.0228e-02	1.74	1.7527e-01	0.78
1/8	2.5351e-03	2.01	8.5201e-02	1.04
1/16	6.2420e-04	2.02	4.1596e-02	1.03

TABLE 7. The CPU time under different grid size in the two-dimensional case.

h	$\|p - p_h\|_0$	Rate	CPU time	$\|p - p_d\|_0$	Rate	CPU time
1/2	3.6152e-02	0	0.53	3.3752e-02	0	0.27
1/4	1.2567e-02	1.52	2.06	1.1755e-02	1.52	0.40
1/8	4.4187e-03	1.51	9.82	4.1394e-03	1.50	1.01
1/16	1.5558e-03	1.51	57.68	1.4548e-03	1.51	6.32
1/32	5.4862e-04	1.50	353.42	5.1208e-04	1.51	32.68
1/64	1.9345e-04	1.50	3184.57	1.8012e-04	1.51	125.33

TABLE 8. The CPU time under different grid size in the three-dimensional case.

h	$\|p - p_h\|_0$	Rate	CPU time	$\|p - p_d\|_0$	Rate	CPU time
1/2	2.1696e-01	0	1.00	2.1696e-01	0	1.05
1/4	7.1250e-02	1.60	2.28	4.1141e-02	2.40	4.48
1/8	2.0851e-02	1.77	84.58	1.2623e-02	1.70	26.63
1/16	6.4503e-03	1.69	2311.35	3.7604e-03	1.75	312.05

source functions are expressed as follows in two dimensions:

$$\boldsymbol{f} = \begin{bmatrix} -(x-6)e^{-7\sqrt{(x-6)^2+(y-6)^2}} \\ -(y-6)e^{-7\sqrt{(x-6)^2+(y-6)^2}} \end{bmatrix} g(t),$$

TABLE 9. The CPU time under different record time with $h = 1/32$ in the two-dimensional case.

Record time (s)	$\|u - u_h\|_0$	CPU time	$\|u - u_d\|_0$	CPU time
1	2.3226e-06	353.42	2.1912e-06	32.68
2	2.5111e-06	591.20	2.3376e-06	76.73
3	2.9776e-07	1072.47	2.6511e-07	130.69
4	2.0809e-06	1393.61	1.9765e-06	195.17
5	2.6840e-06	1919.23	2.4332e-06	280.32

TABLE 10. The CPU time under different record time with $h = 1/8$ in the three-dimensional case.

Record time (s)	$\|u - u_h\|_0$	CPU time	$\|u - u_d\|_0$	CPU time
1	8.90201e-04	52.64	8.79000e-04	17.36
2	9.62345e-04	137.21	9.55745e-04	68.97
3	1.48971e-04	248.36	1.46846e-04	101.55
4	8.02991e-04	394.06	8.00694e-04	165.03
5	5.85106e-04	568.07	5.64295e-04	318.45

and expressed as follows in three dimensions:

$$\boldsymbol{f} = \begin{bmatrix} -(x-6)e^{-7\sqrt{(x-6)^2+(y-6)^2+(z-6)^2}} \\ -(y-6)e^{-7\sqrt{(x-6)^2+(y-6)^2+(z-6)^2}} \\ -(z-6)e^{-7\sqrt{(x-6)^2+(y-6)^2+(z-6)^2}} \end{bmatrix} g(t),$$

where $g(t) = 2a(2a(t-b)^2-1)e^{-a(t-b)^2}$, $a = (\frac{\pi}{1.31})^2$ and $b = 1.35$. The computation area in two dimensions is $[12 \times 12]$, and the computation area in three dimensions is $[12 \times 12 \times 12]$. The mesh size is $h = 6/25$ in two dimensions, and the mesh size is $h = 3/5$ in three dimensions. The time step is $\Delta t = 0.001s$, and the record time is $T = 1s$. In addition, $\lambda = 1$, $\mu = 1$, $\rho = 1$ and $L = 500$.

We compare the graphs of the two methods in Figures 1-2, and the results show that the solutions obtained by the POD-ROM are not significantly different from those obtained by the FOM. Furthermore, in the three-dimensional example, we intercepted the waveform diagram of the plane at $x = 6$, as shown in Figure 3. The waveform diagram of the POD-ROM matches well with that of the FOM. At the same time, we recorded the time required for the POD-ROM and the FOM and the number of POD bases d selected in Table 11. It can be seen that the calculation time of the POD-ROM is significantly less than that of the FOM while maintaining accuracy.

5.4. Wave propagation. To further investigate the FOM and the POD-ROM, we simulated the propagation of two-dimensional wave in this subsection. The computational area is $[0, 100] \times [0, 100]$ and the space step is $h = 1$. The time step is $\Delta t = 0.001s$, and the record time is $T = 1s$. The source term is located at $(50, 100)$, and it has form $f = \sin(2\pi f_0)exp(-\pi^2 f_0^2 t^2/4)$ where $f_0 = 30$. In addition, the initial value and the boundary value are zero.

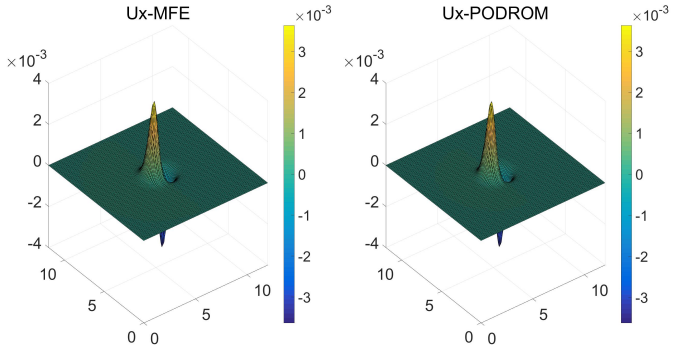

(A) Displacement U_x

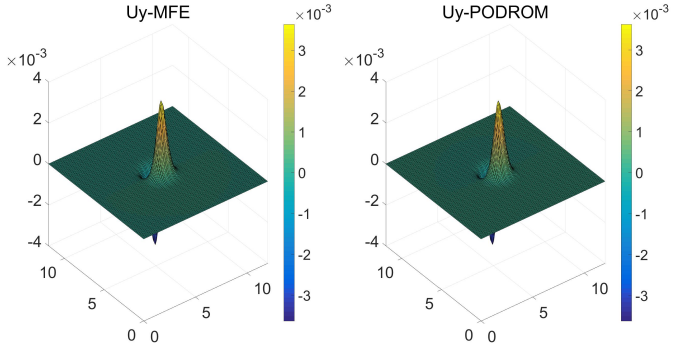

(B) Displacement U_y

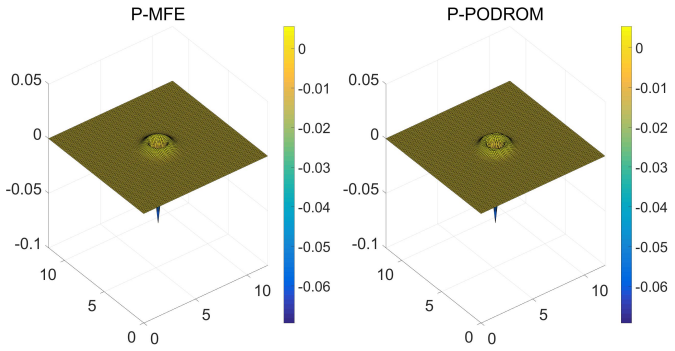

(C) Pseudo-pressure P

FIGURE 1. Comparison of surface graphs of the FOM and the POD-ROM method at $T = 1s$ in 2D numerical test.

We tested and simulated the propagation of waves in a homogeneous medium model and a two-layer model. The parameters of the homogeneous medium model are $\lambda = 10000$, $\mu = 10000$, and $\rho = 1$. In the two-layer model, the interface is set at $y = 50$, the parameters of the upper layer are $\lambda = 10000$, $\mu = 10000$ and $\rho = 1$, the parameters of the lower layer are $\lambda = 1000$, $\mu = 1000$ and $\rho = 1$. We record the snapshots at different time, as shown in Figure 4-5. In the POD model reduction algorithm, we set the number of sample snapshots $L = 600$.

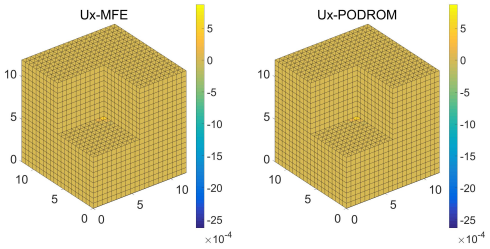

(A) Displacement U_x

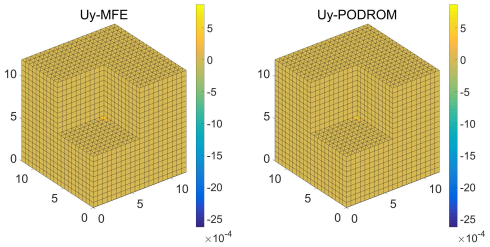

(B) Displacement U_y

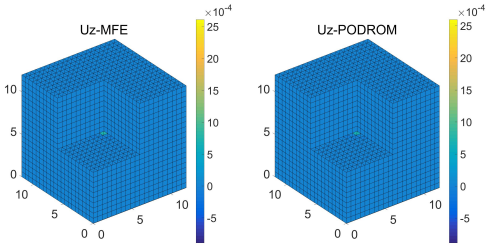

(C) Displacement U_z

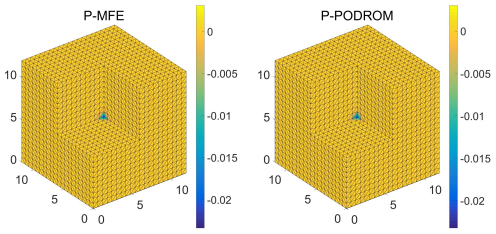

(D) Pseudo-pressure P

FIGURE 2. Comparison of surface graphs of the FOM and the POD-ROM method at $T = 1s$ in 3D numerical test.

Figure 4 shows that the MFE method simulates wave propagation very well, and the POD method is also effective. Figure 5 shows that the wave is reflected at the interface. Moreover, when we compare the computational time of the FOM and the POD-ROM in Table 12, the results show that the computational efficiency of the POD-ROM is slightly higher.

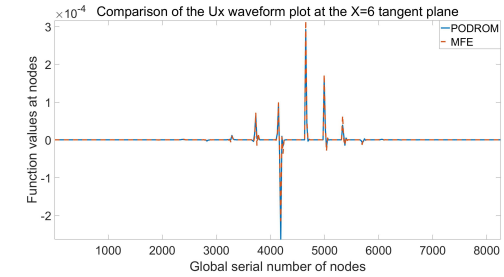

(A) Displacement U_x

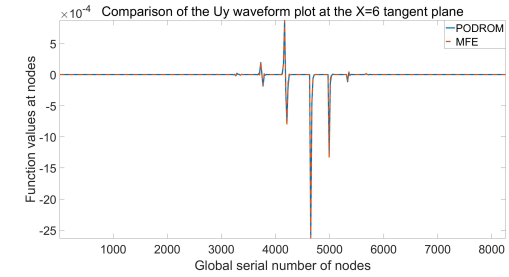

(B) Displacement U_y

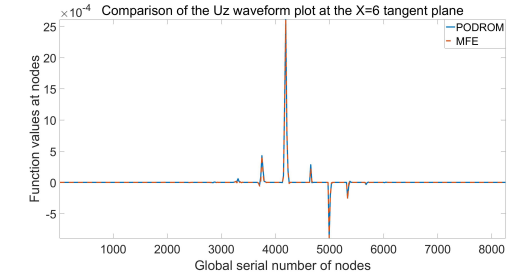

(C) Displacement U_z

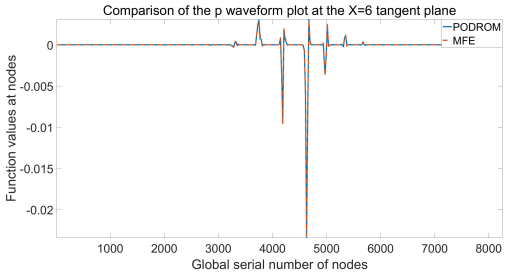

(D) Pseudo-pressure P

FIGURE 3. Comparison of the waveforms of the FOM and the POD-ROM method at tangent plane $x = 6$.

6. Conclusions

In this paper, we give a locking-free ROM to solve the elastic wave equation. First, we use the locking-free mixed finite element method to construct an FOM, and then we use the POD technique to construct a ROM called POD-ROM. In this way, the POD-ROM can greatly improve the computing efficiency compared

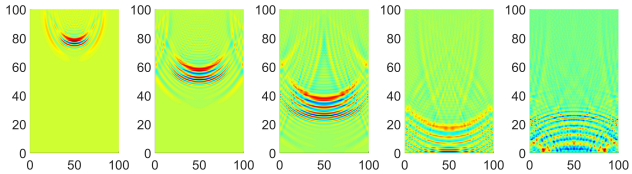

(A) Displacement U_x of FOM

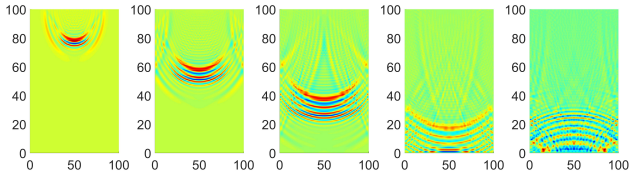

(B) Displacement U_x of POD-ROM

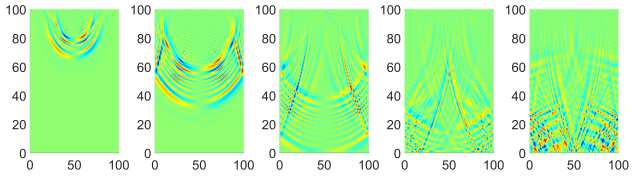

(C) Displacement U_y of FOM

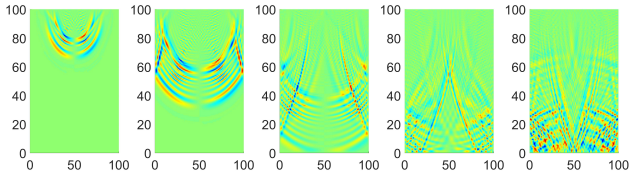

(D) Displacement U_y of POD-ROM

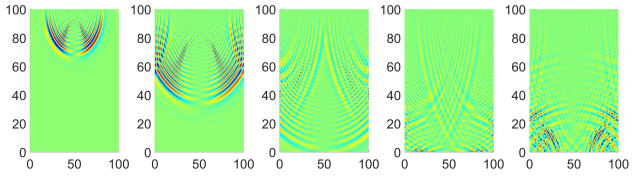

(E) Pseudo-pressure P of FOM

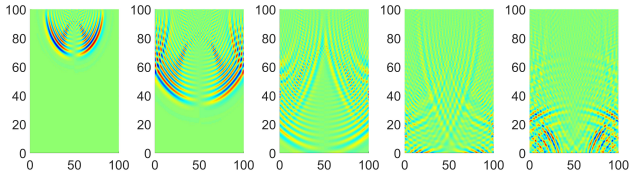

(F) Pseudo-pressure P of POD-ROM

FIGURE 4. Snapshots of the homogeneous medium model obtained using FOM and POD-ROM methods recorded at different times $T = 0.2s, 0.4s, 0.6s, 0.8s, 1.0s$.

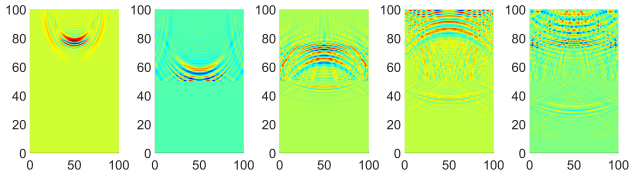

(A) Displacement U_x of FOM

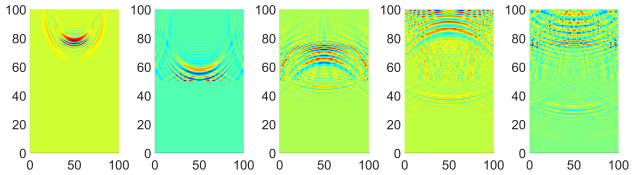

(B) Displacement U_x of POD-ROM

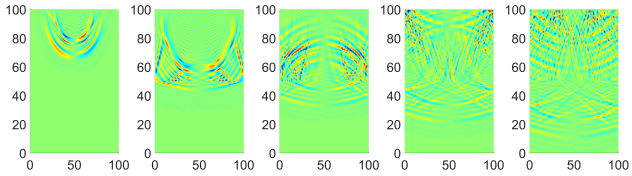

(C) Displacement U_y of FOM

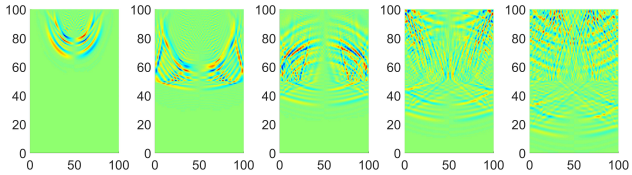

(D) Displacement U_y of POD-ROM

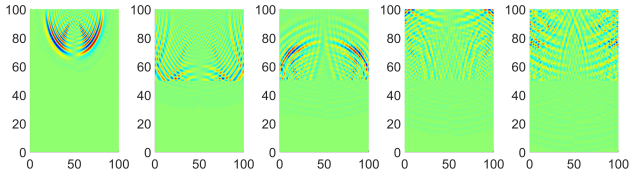

(E) Pseudo-pressure P of FOM

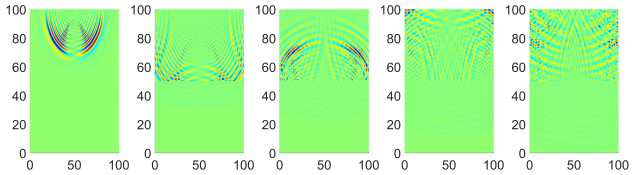

(F) Pseudo-pressure P of POD-ROM

FIGURE 5. Snapshots of the two-layer model obtained using FOM and POD-ROM methods recorded at different times $T = 0.2s, 0.4s, 0.6s, 0.8s, 1.0s$.

Table 11. Comparison of CPU Time.

Dimension	CPU Time (s) using FOM	CPU Time (s) using POD-ROM	d
2	1453	351	5
3	7340	1432	6

Table 12. Comparison of CPU Time.

Dimension	CPU Time (s) using FOM	CPU Time (s) using POD-ROM
2	3658	2218

with the FOM while maintaining the characteristics of numerical accuracy and locking-free. In addition, the solution of parameterized partial differential equations (PDEs) plays a crucial role in various fields of scientific and engineering computation. These problems are often encountered in the modeling of complex physical systems, where multiple parameters (such as material properties or external forces) significantly affect the system's behavior. However, solving such systems in full can be computationally expensive, especially when simulations need to be repeated for a large number of different parameter values. Model reduction methods have become widely used in these contexts due to their ability to significantly reduce computational complexity while maintaining a high level of accuracy. Among these methods, Proper Orthogonal Decomposition (POD) is a popular technique that generates a low-dimensional approximation of the system by extracting the most relevant features from a set of simulation snapshots. In the future, we will further use the POD-ROM for practical engineering problems and study the model reduction methods for solving parameterized PDEs.

Acknowledgments

This research is supported by the National Natural Science Foundation of China (No. 11971337). The author thanks the reviewers and editors for their careful review.

References

[1] Becache E, Joly P, Tsogka C. Fictitious domains, mixed finite elements and perfectly matched layers for 2-D elastic wave propagation. Journal of Computational Acoustics, 2001, 9(03): 1175-1201.

[2] Marfurt K J. Accuracy of finite-difference and finite-element modeling of the scalar and elastic wave equations . Geophysics, 1984, 49(5): 533-549.

[3] Wu S R. A priori error estimates for explicit finite element for linear elasto-dynamics by Galerkin method and central difference method. Computer Methods in Applied Mechanics and Engineering, 2003, 192(51-52): 5329-5353.

[4] Sern F J, Sanz F J, Kindelan M, et al. Finite-element method for elastic wave propagation . Communications in Applied Numerical Methods, 1990, 6(5): 359-368.

[5] Dauksher W, Emery A F. The solution of elastostatic and elastodynamic problems with Chebyshev spectral finite elements. Computer Methods in Applied Mechanics and Engineering, 2000, 188(1-3): 217-233.

[6] Zyserman F I, Gauzellino P M, Santos J E. Dispersion analysis of a nonconforming finite element method for the Helmholtz and elastodynamic equations. International Journal for Numerical Methods in Engineering, 2003, 58(9): 1381-1395.

[7] De Basabe J D, Sen M K, Wheeler M F. The interior penalty discontinuous Galerkin method for elastic wave propagation: grid dispersion. Geophysical Journal International, 2008, 175(1): 83-93.
[8] K?ser M, Dumbser M. An arbitrary high-order discontinuous Galerkin method for elastic waves on unstructured meshesI. The two-dimensional isotropic case with external source terms. Geophysical Journal International, 2006, 166(2): 855-877.
[9] Mercerat E D, Glinsky N. A nodal high-order discontinuous Galerkin method for elastic wave propagation in arbitrary heterogeneous media. Geophysical Journal International, 2015, 201(2): 1101-1118.
[10] Berkooz G, Holmes P, Lumley J L. The proper orthogonal decomposition in the analysis of turbulent flows. Annual Review of Fluid Mechanics, 1993, 25(1): 539-575.
[11] Kunisch K, Volkwein S. Galerkin proper orthogonal decomposition methods for parabolic problems. Numerische mathematik, 2001, 90: 117-148.
[12] Hesthaven J S, Rozza G, Stamm B. Certified reduced basis methods for parametrized partial differential equations. Berlin: Springer, 2016.
[13] Quarteroni A, Manzoni A, Negri F. Reduced basis methods for partial differential equations: an introduction. Springer, 2015.
[14] Luo Z, Chen J, Navon I M, et al. Mixed finite element formulation and error estimates based on proper orthogonal decomposition for the nonstationary Navier-Stokes equations. SIAM Journal on Numerical Analysis, 2009, 47(1): 1-19.
[15] Li X, Luo Y, Feng M. An Efficient Chorin-Temam Projection Proper Orthogonal Decomposition Based Reduced-Order Model for Nonstationary Stokes Equations. Journal of Scientific Computing, 2022, 93(3): 64.
[16] Luo Z, Xie Z, Shang Y, et al. A reduced finite volume element formulation and numerical simulations based on POD for parabolic problems . Journal of Computational and Applied Mathematics, 2011, 235(8): 2098-2111.
[17] Luo Z, Chen G. Proper orthogonal decomposition methods for partial differential equations. Academic Press, 2018.
[18] Luo Z, Jin S. A reduced-order extrapolated Crank-Nicolson collocation spectral method based on proper orthogonal decomposition for the two-dimensional viscoelastic wave equations . Numerical Methods for Partial Differential Equations, 2020, 36(1): 49-65.
[19] Luo Z, Jiang W. A reduced-order extrapolated technique about the unknown coefficient vectors of solutions in the finite element method for hyperbolic type equation. Applied Numerical Mathematics, 2020, 158: 123-133.
[20] Douglas J, Gupta C P. Superconvergence for a mixed finite elmenent method for elastic wave propagation in a plane domain. Numerische Mathematik, 1986, 49: 189-202.
[21] Makridakis C G. On mixed finite element methods for linear elastodynamics. Numerische Mathematik, 1992, 61(1): 235-260.
[22] Bcache E, Joly P, Tsogka C. A new family of mixed finite elements for the linear elastodynamic problem. SIAM Journal on Numerical Analysis, 2002, 39(6): 2109-2132.
[23] Arnold D N, Lee J J. Mixed methods for elastodynamics with weak symmetry. SIAM Journal on Numerical Analysis, 2014, 52(6): 2743-2769.
[24] Brezzi F, Fortin M. Mixed and hybrid finite element methods. Springer Science Business Media, 2012.
[25] Jenkins E W, Rivire, B, Wheeler M F. A priori error estimates for mixed finite element approximations of the acoustic wave equation. SIAM Journal on Numerical Analysis, 2002, 40(5): 1698-1715.
[26] Li J, He Y, Chen Z. A new stabilized finite element method for the transient Navier-Stokes equations. Computer Methods in Applied Mechanics and Engineering, 2007, 197(1-4): 22-35.
[27] Arnold D N, Brezzi F, Fortin M. A stable finite element for the Stokes equations . Calcolo, 1984, 21(4): 337-344.
[28] Cowsar L C, Dupont T F, Wheeler M F. A priori estimates for mixed finite element approximations of second-order hyperbolic equations with absorbing boundary conditions. SIAM Journal on Numerical Analysis, 1996, 33(2): 492-504.
[29] Jenkins E W. Numerical solution of the acoustic wave equation using Raviart-Thomas elements. Journal of Computational and Applied Mathematics, 2007, 206(1): 420-431.

Department of Mathematics, Sichuan University, Chengdu, China, 610065
E-mail: 530441397@qq.com

Department of Mathematics, Sichuan University, Chengdu, China, 610065
E-mail: xyc@scu.edu.cn and fmf@scu.edu.cn